Passive Crowd Buffering in Pre-Operational Transit Stations: A Hybrid Simulation Study of the Thammasat University SRT Red Line Station

Lik Ren Tai[a]*, Chairat Muksri[b]

[a] *Woosong University, Daejeon, Korea (ORCID iD: 0009-0002-6667-3331)*
[b] *Electrified Rail Management Bureau, State Railway of Thailand, Bangkok, Thailand*

Abstract

The planned Thammasat University station on the State Railway of Thailand's Red Line Phase II extension presents a pre-operational evaluation challenge common to transit-oriented stations serving university catchments: demand assumptions and resilience claims must be established before the station exists to validate them against. This study addresses that challenge through a dual-tier hybrid simulation, a macroscopic Machinations Discrete Event Simulation cross-validated against a microscopic AnyLogic pedestrian model, stress-tested across six scenarios spanning baseline operation, hardware degradation, network disruption, and impulse loading. The central finding is that the station's Skywalk Concourse functions as a passive crowd buffer: under both the most severe internal failure (escalator loss, 446 passengers) and an extreme exogenous load (a 1,500-passenger stadium egress, 415 passengers), the concourse absorbs spatial accumulation that would otherwise reach the platform, remaining within Pedestrian Level of Service B in every case. This buffering capacity, however, was tested against demand assumptions that this study finds to be conservative. Empirical validation against twelve months of origin-destination data from the existing thirteen-station network shows that all operating stations, including the two closest behavioural proxies for Thammasat, exceed the simulation's assumed peak-hour k-factors (12% AM, 10% PM) by 26 to 70%, with an empirically grounded range of 15 to 20% AM and 12 to 15% PM proposed for future scenario refinement. Station typology classification further shows that the two proxy stations fall into structurally different demand archetypes, indicating that network position rather than university-adjacency alone governs temporal demand concentration. Finally, Heat Index projections to 2050, anchored to an ERA5 baseline and a three-model CMIP6 ensemble, suggest a climatically-driven catchment-shrinkage mechanism that could render the concentrated-demand conditions already modelled closer to typical than exceptional by mid-century under high-emissions pathways. Together, these findings suggest that passive architectural width, not solely active crowd management, may represent a transferable resilience parameter for transit-oriented station design, warranting investigation across additional station typologies.

Keywords: Transit-oriented development; pre-operational simulation; pedestrian level of service; hybrid discrete-event simulation; station typology classification; Heat Index; climate stress-testing; SRT Red Line

---

1. Introduction

Rapid urbanisation across Southeast Asia is placing growing pressure on metropolitan transit authorities to deliver infrastructure that is not only physically adequate but operationally resilient under real-world conditions. In Thailand, the State Railway of Thailand (SRT) Red Line commuter network forms a central pillar of this effort, with Phase 1 covering 26.30 km between the Krung Thep Aphiwat Central Terminal and Rangsit since late 2021 [1]. Phase II extends the line a further 8.84 km north from Rangsit, explicitly to serve Thammasat University (Rangsit Campus) and the surrounding Pathum Thani residential zones, with construction contracts signed in May 2026 and works expected to begin in July 2026 [2]. Unlike conventional commercial nodes, a university-adjacent station functions as a specialised transit-oriented development anchor, generating severe,

time-specific peak-hour surges tied to academic schedules and placing immense localised pressure on ingress points, ticketing queues, and platform areas [3].

Because Phase II remains pre-operational, conventional feasibility assessments, which rely on static demand models and fixed capacity figures, are insufficient for guiding operational policy ahead of service launch. Such assessments cannot capture how queues form and dissipate at fare-gates, how platform crowding evolves across a peak hour, or how spatial friction redistributes load across a station's access infrastructure. This leaves operators without an evidence base for decisions on service frequency or targeted infrastructure reinforcement.

Climatic conditions compound this gap. In tropical contexts, elevated Heat Index, humidity, and seasonal monsoons are known to compress the effective walking distance commuters are willing to tolerate, altering the distance-decay parameters that underpin catchment-area estimates derived from temperate-climate research [4]. For a station whose architecture and access topology are still subject to design refinement, understanding how these climatic pressures interact with passenger demand and station infrastructure is a planning-relevant question, not merely an academic one.

This study addresses these gaps through a dual-tier hybrid simulation methodology, combining a macroscopic Discrete Event Simulation in Machinations with a microscopic, continuous-physics 3D pedestrian simulation in AnyLogic. A modified gravity model translates the station's 13-zone catchment area into a calibrated peak-hour demand profile, which is then subjected to six stress-test scenarios spanning baseline operation, localised hardware failure, and network-level or impulse-load disruptions. The two simulation tiers are cross-validated against one another, and peak-hour demand assumptions are further checked against an empirical origin-destination dataset drawn from comparable stations on the existing network.

Three contributions follow from this approach. First, the cross-tier cross-validation and stress-testing identify the station's Skywalk Concourse as functioning as a passive crowd buffer: under both localised hardware failure and severe impulse-load conditions, the concourse absorbs substantial spatial accumulation while the platform remains within acceptable service levels, a structural property with direct implications for station design and crowd management. Second, an empirical validation against operational origin-destination data from comparable stations, together with a typological classification exercise, situates the Thammasat archetype within a broader family of university-adjacent and terminus-like station profiles, supporting generalisation of the findings beyond this single site. Third, the study extends the operational analysis into the climate domain, using Heat Index projections to 2050 derived from ERA5 reanalysis and a three-model CMIP6 ensemble to propose a climatically-driven catchment-shrinkage mechanism, linking projected warming trends to the demand-concentration conditions already explored in the impulse-load scenarios.

The remainder of this paper is organised as follows. Section 2 reviews the relevant literature on transit catchment modelling, pedestrian dynamics under climatic friction, and hybrid simulation paradigms. Section 3 describes the study area, data sources, and simulation methodology. Section 4 presents the results, covering the demand baseline and cross-validation, the Skywalk Concourse buffering finding, empirical validation of demand assumptions, station typology and archetype classification, and the climate stress-testing analysis. Section 5 discusses the implications of these findings for station design and operational policy, and Section 6 concludes with a summary of contributions, limitations, and directions for future work.

2. Literature Review

This review situates the present study within five bodies of literature. The first three, transit-oriented development and catchment-area theory, pedestrian dynamics and climatic impedance, and computational simulation paradigms, underpin the dual-tier simulation methodology and were the basis of the original thesis. The remaining two, empirical demand validation and station typology, and the climate science of Heat Index

projection, support the expanded empirical-validation, archetype-generalisation, and climate stress-testing analyses presented in Section 4.

2.1 Transit-oriented development, catchment areas, and the Gravity Model

The integration of land use and transit infrastructure is encapsulated by the paradigm of Transit-Oriented Development (TOD), originally formalised by Calthorpe [5] and widely adopted in developing economies as a mechanism to curb sprawl and maximise the viability of rail investment [6]. For major institutional anchors, a station functions not merely as an access point but as a primary spatial attractor shaping regional commuter behaviour [7], making the precise evaluation of station capacity inseparable from the density and distribution of the development it serves.

Catchment-area definitions have evolved correspondingly. Static Euclidean buffers of 500 to 800 m, long the planning default, are now understood to overestimate true pedestrian access, particularly in suburban or geographically constrained settings [8]. Network-based accessibility measures, accounting for actual pedestrian infrastructure such as sidewalks, skywalks, and crossings, better capture how physical barriers and fragmented street networks channel passenger movement toward specific architectural entry points [9].

Quantifying travel demand within such catchments relies on the Gravity Model of Spatial Interaction, originating in Zipf's application of Newtonian analogy to human movement [10], later adapted for urban accessibility by Hansen [11] and formalised into its modern entropy-maximising form by Wilson [12]. In this formulation, trip volume between an origin and destination is proportional to their respective masses and inversely related to a distance-decay parameter (β) representing pedestrian reluctance to travel. Calculating this β term for tropical climates, and using it to allocate arriving passenger volumes to specific station exits, provides the foundational demand input for the discrete-event simulations described in Section 3 [4].

2.2 Pedestrian dynamics and climatic impedance on walkability

Macroscopic demand models predict approach volumes, but congestion at a station is governed by microscopic pedestrian movement and local environmental conditions. Fruin's foundational work established the concept of pedestrian Level of Service (LOS), demonstrating that walking speed deteriorates sharply as crowd density increases within confined spaces [13]. This deterioration is most pronounced at chokepoints such as fare gates, escalators, and platform boarding zones, where capacity is highly stochastic and influenced by individual behaviour, luggage, and bidirectional conflicts [14], a stochasticity that static capacity calculations cannot capture.

A further limitation of standard spatial models is the assumption of uniform distance-decay parameters. Foundational walking-distance thresholds of 400 to 800 m were calibrated predominantly using temperate-climate data from Europe, North America, and Australia [15]. In tropical contexts, however, heat, humidity, and seasonal monsoons substantially compress the distance commuters are willing to walk. Empirical work on Bangkok-area commuters confirms that acceptable walking distance drops markedly under direct sun and elevated temperature [4], with stated-preference studies indicating that students are unlikely to walk more than approximately 400 m under such conditions [16]. The β parameter used in the Gravity Model for the SRT Red Line must therefore be adjusted to reflect this climatic impedance.

Built-environment quality moderates this effect. High-quality, weather-protected pedestrian infrastructure, continuous sidewalks, crosswalks, and shaded or elevated skywalks, flattens the distance-decay curve and expands a station's functional catchment without altering its physical location [17]. For a university-adjacent station such as Thammasat, the presence of such infrastructure, and specifically its role in absorbing concentrated pedestrian flows under both routine and extreme conditions, is a structural property that this study examines directly (Section 4.2).

2.3 Computational simulation paradigms

Static Geographic Information System (GIS) mapping can define where passengers originate but cannot represent dynamic movement or time-based operational failure, such as the cascading congestion that follows a turnstile failure during a peak surge. Discrete Event Simulation (DES) addresses this by modelling system state as a chronological sequence of discrete events, such as a fare-gate tap or a train boarding [18], and has been applied successfully to model passenger flow through architectural chokepoints by assigning processing-time distributions to individual conditions [19].

To manage the complexity of DES models and make them accessible for pre-operational decision-making, visual node-based frameworks rooted in Petri Net theory [20] are increasingly used. Such frameworks represent passenger flow as resource tokens moving through a visible network of places and transitions, in contrast to the comparatively opaque code-based representations of conventional microscopic simulation tools. This visual paradigm supports rapid, pre-operational A/B testing without requiring extensive programming expertise from the policymakers who must interpret the results.

Deterministic models, however, assume average conditions and cannot represent the unpredictability of real-world operations. Monte Carlo methods address this by introducing stochastic variation across thousands of iterations, allowing simulations to account for train delays, hardware failures, and demand surges, and thereby establishing whether a station's architecture remains resilient under worst-case conditions [21]. This study adopts a dual-tier approach in this spirit, pairing a macroscopic, Petri Net-based Discrete Event Simulation (Machinations) with a microscopic, continuous-physics 3D pedestrian simulation (AnyLogic), cross-validated against one another to combine the interpretability of the former with the behavioural fidelity of the latter.

2.4 Empirical demand validation and station typology

A persistent limitation of pre-operational simulation is that gravity-model demand assumptions and stress-test k-factors are typically calibrated without reference to observed operational data, since the station in question does not yet exist. One response is to validate these assumptions against operational data from structurally comparable existing stations, an approach consistent with the broader use of analogous-site benchmarking in transit demand forecasting [22]. This study applies this logic by drawing on a twelve-month origin-destination dataset from the existing SRT Red Line Phase I network to test whether the peak-hour k-factors assumed in the Machinations model are consistent with observed peaking behaviour at proxy stations selected for network position and adjacent land use.

A second response, station typology, classifies stations into demand-based archetypes using clustering methods applied to standardised peaking metrics, allowing a station that does not yet exist to be positioned within a family of structurally similar stations whose behaviour is already observed [23]. K-means clustering on temporal demand-shape features, with and without absolute demand volume as an additional dimension, is a widely used approach for this purpose in transit planning contexts and underpins the archetype classification presented in Section 4.4.

2.5 Climate science for transit infrastructure: Heat Index and CMIP6 projections

Linking climatic impedance (Section 2.2) to future operational conditions requires projecting how the thermal environment around a station will change over coming decades. The Heat Index, most commonly computed via the Rothfusz regression from near-surface air temperature and relative humidity, provides a standard measure of perceived thermal stress that is more behaviourally relevant than air temperature alone, particularly in humid tropical settings [24].

Historical baselines for such projections are commonly derived from atmospheric reanalysis products such as ERA5, which assimilate observations to provide spatially continuous, observationally-constrained estimates of past climate [25]. Future trends are derived from Coupled Model Intercomparison Project Phase 6 (CMIP6)

global climate models under standardised Shared Socioeconomic Pathway (SSP) emissions scenarios, which provide a range of plausible future trajectories for temperature and humidity [26]. A well-documented limitation of applying CMIP6 output to small, tropical, urban areas is a systematic cool and dry bias relative to reanalysis, arising from coarse spatial resolution, the absence of urban heat island parameterisation, and over-represented convective mixing in tropical regions [27]. Established practice in climate impact assessment is to treat such offsets as a methodological limitation to be reported explicitly, using reanalysis for the absolute baseline and climate-model output for the direction and rate of future change, rather than applying ad hoc bias correction [27]. This framing underpins the climate stress-testing approach adopted in Section 4.5.

2.6 Summary and methodological justification

Three gaps in the literature are directly relevant to this study: the absence of empirical validation of pre-operational demand assumptions against operational data from comparable stations; the limited application of station typology methods to positioning a not-yet-operational station within an existing network's demand archetypes; and the gap between established climatic-impedance findings and forward-looking projections linking climate-model output to specific operational stress-test scenarios. This study addresses all three by combining a cross-validated dual-tier simulation with empirical demand benchmarking, archetype classification, and Heat Index projection to 2050.

3. Methodology

3.1 Research framework

The methodology is structured in four sequential tiers. The first translates static spatial and demographic data into a calibrated peak-hour demand profile via a Modified Gravity Model. The second injects this demand profile into a Machinations macroscopic Discrete Event Simulation (DES), whose outputs are cross-validated against a localized AnyLogic microscopic 3D pedestrian simulation. The third tier subjects the cross-validated model to six stress-test scenarios spanning baseline operation, hardware degradation, network disruption, and impulse loading. The fourth tier extends the analysis in two directions beyond the simulation core: an empirical validation of demand assumptions against twelve months of operational origin-destination data from comparable existing stations, and a climate stress-testing analysis linking projected Heat Index trajectories to the demand-concentration conditions explored in the simulation.

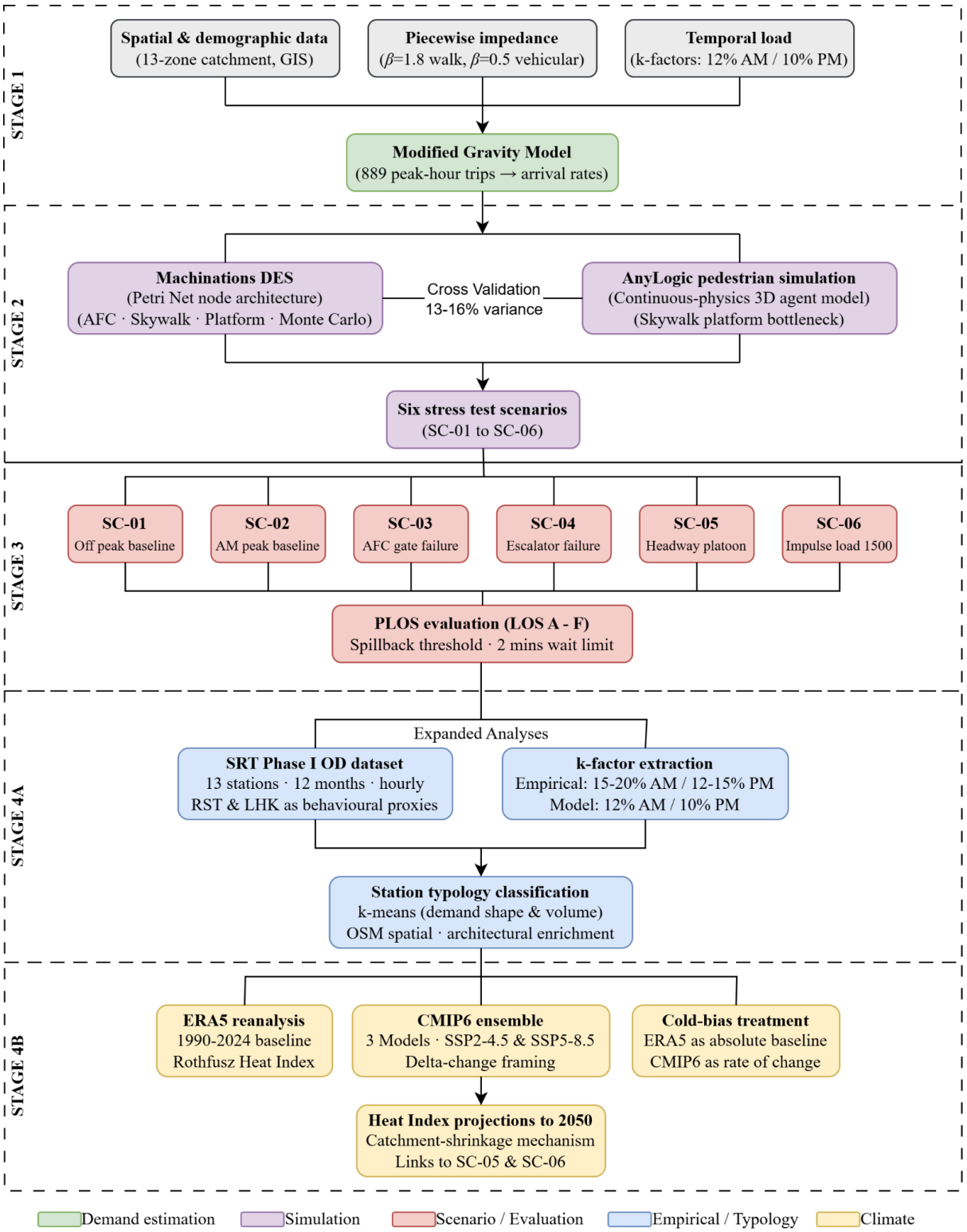

Figure 1. *Methodology workflow showing the four-tier research framework: demand estimation via the Modified Gravity Model (Stage 1), dual-tier simulation cross-validation between Machinations and AnyLogic (Stage 2), six stress-test scenarios with PLOS evaluation (Stage 3), and the two parallel expanded analyses, empirical validation and station typology classification (Stage 4A), and Heat Index climate stress-testing (Stage 4B)*

3.2 Study area

The study concerns the planned Thammasat University station, the future northern terminus of the SRT Red Line Phase II extension (station code RN11/RW01, Pathum Thani Province). The station is elevated, with two entrance gates (east and west), a 130 m × 7 m centre platform, twelve Automatic Fare Collection (AFC) gates, three lifts, and six escalators connecting the platform level to the Skywalk Concourse above. Train headway under the Phase II service plan is 20 minutes. The station's catchment extends across a 13-zone delineation, with zones 1 to 8 covering the predominantly residential western sectors and zones 9 to 13 the eastern sectors comprising Thammasat University (academic core, hospital), the Asian Institute of Technology (AIT), and adjacent residential development. The eastern boundary is defined by the university campus; the northern and southern boundaries are set at the midpoints to the nearest stations (Nava Nakorn to the north and Chiang Rak to the south). The 13-zone catchment, including the irregular boundaries and station origin node used for Gravity Model distribution, is shown in Figure 2.

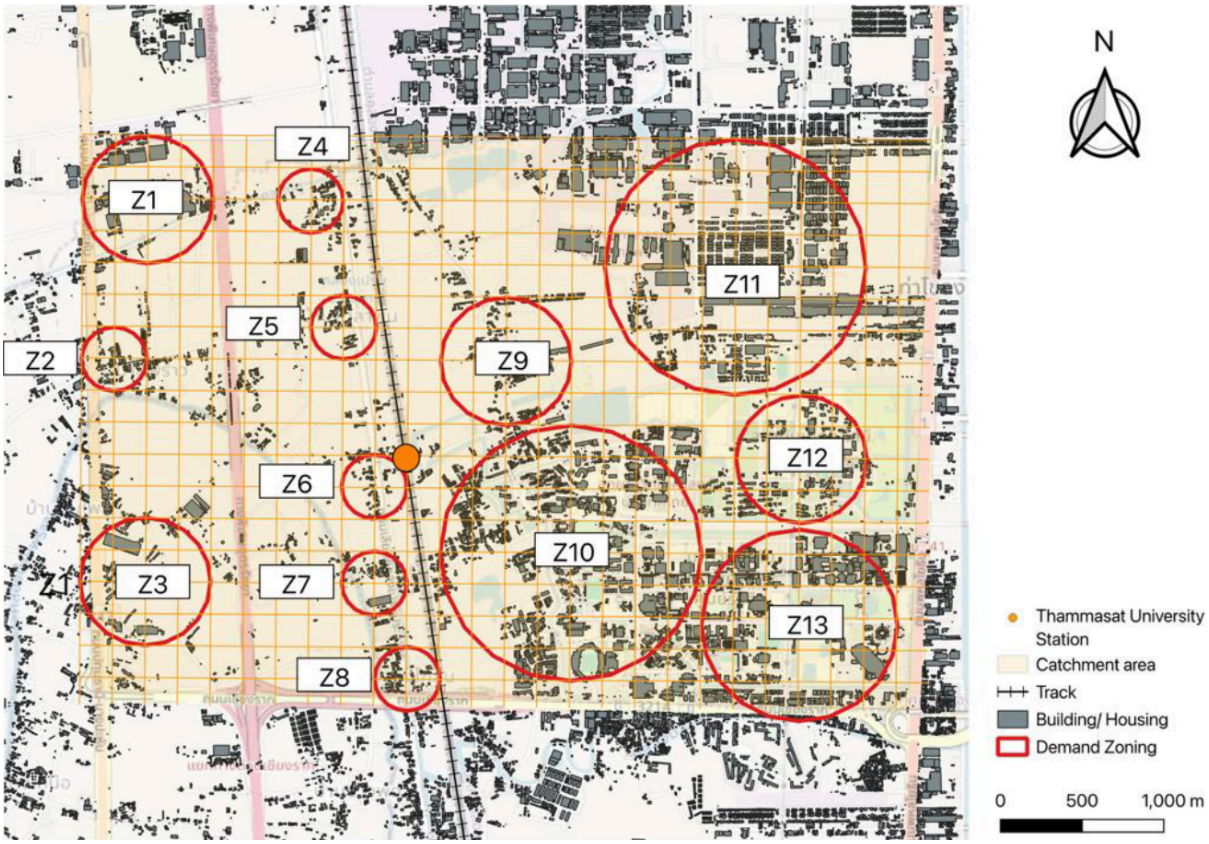

Figure 2. *Spatial demand zoning (Z1 to Z13) and the station origin node used for Modified Gravity Model trip distribution. Zone boundaries reflect the catchment's irregular density and land-use distribution rather than uniform radial buffers.*

3.3 Modified Gravity Model and demand estimation

3.3.1 Model specification and catchment zoning

Peak-hour trip generation from each zone i to the station is estimated using a Modified Gravity Model:

$$T_{ij} = P_i \times P_d(d_{ij})$$

where P_i is the population or enrolment-derived passenger-generating mass of zone i (in passengers per km²), and $P_d(d_{ij})$ is a distance-decay impedance function, a dimensionless multiplier between 0 and 1 representing the

probability that a trip is undertaken given the distance d_{ij} from zone i to the station, evaluated at the centroid distance and not itself a population or mass term despite the shared notation.

The Machinations source nodes for each catchment zone were spatially organised against an underlying GIS map of the station catchment to aid model interpretability and verify the geographic plausibility of the zone-to-station relationships (Figure 3), although the distance parameter (d) used in the impedance function was derived from randomised sampling within each zone's spatial boundary rather than measured path length.

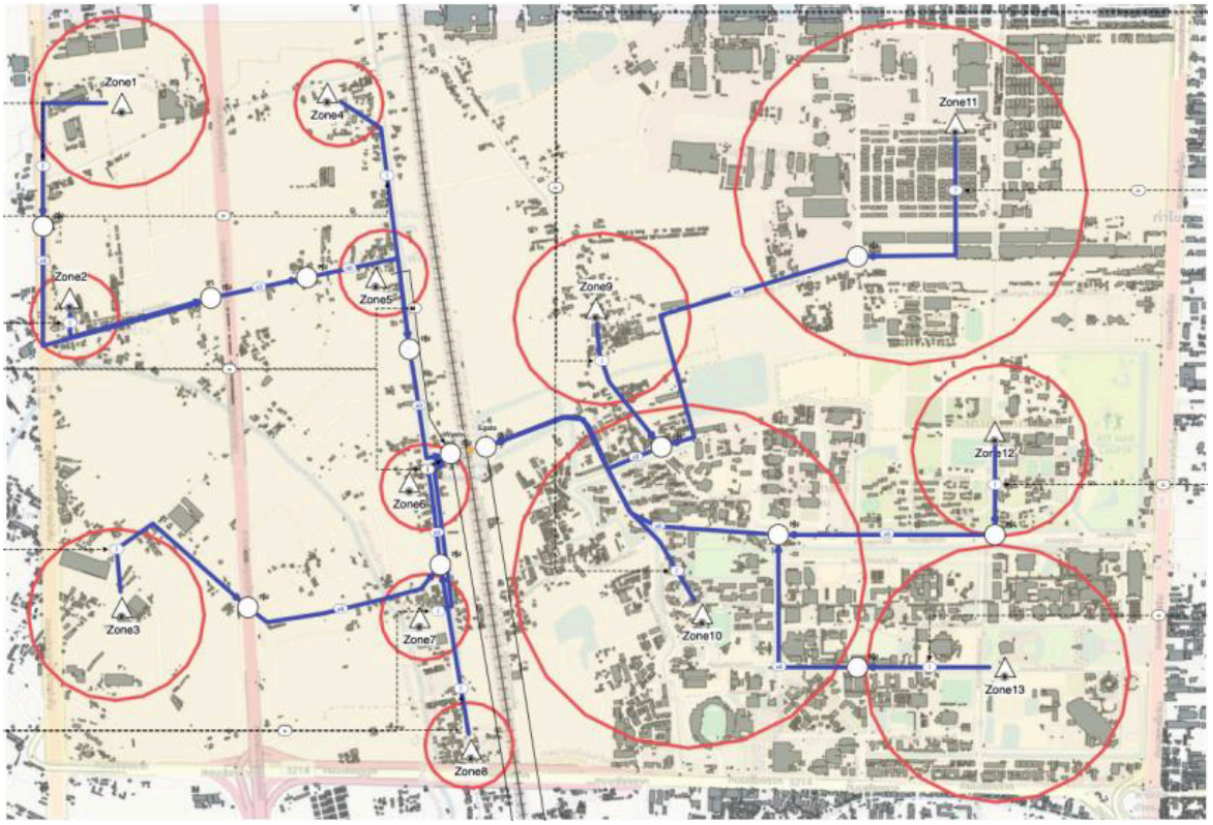

***Figure 3**. Spatial organisation of the Modified Gravity Model source nodes for each catchment zone (Z1 to Z13), overlaid on the station catchment GIS map. Node positions and connecting paths reflect the geographic layout of the catchment to support model interpretability; the distance parameter (d) used in the impedance function was derived from randomised sampling within each zone boundary rather than measured along these paths.*

3.3.2 Piecewise climatic impedance function

A fixed β parameter is inappropriate for a tropical university-adjacent catchment in which access mode shifts sharply with distance. This study adopts a piecewise impedance function:

- $P_d = exp(-\beta_{walk} \times d)$ if $d \leq 0.4$ km
- $P_d = exp(-\beta_{transit} \times d)$ if $d > 0.4$ km

For the pedestrian segment, $\beta_{walk} = 1.8$, calibrated to reflect the documented rapid drop-off in walking willingness under Bangkok-area tropical conditions, where empirical stated-preference evidence places the effective walking threshold at approximately 400 m [16]. For the vehicular-feeder segment (campus EV shuttle, motorcycle taxi, songthaew), $\beta_{transit} = 0.5$, reflecting the substantially reduced friction once physical exertion is eliminated. The piecewise formulation captures the behavioural revitalisation of demand at longer distances once motorised access is available. The 400 m breakpoint is taken directly from empirical Bangkok-area data; the β values represent informed transferred assumptions, acknowledged as a limitation in the absence of

pre-operational on-site calibration data. Because β_{walk} is a transferred assumption rather than a site-calibrated parameter, its influence on the Gravity Model's demand output was tested across a representative range (β_{walk} = 1.2, 1.5, 1.8, 2.1, spanning approximately ±17% around the adopted value) via Monte Carlo sampling from the same per-zone distance ranges used in the operational model (10,000 draws per zone per β_{walk} value), with $\beta_{transit}$ and the 400 m breakpoint held fixed.

Across this range, total P_d weighted demand mass varies by less than 3% (corresponding to approximately 878 to 915 peak-hour trips against the published baseline of 889), and the walkable-zone share of total demand shifts only modestly, from approximately 20% at β_{walk} = 1.2 to approximately 17% at β_{walk} = 2.1 (Table 1). This limited sensitivity follows directly from the catchment's geography rather than from any cancellation in the model: of the thirteen zones, only one (Zone 3) lies entirely within the 400 m walkable threshold, five (Zones 4 to 8) are partially walkable, and the remaining seven lie entirely beyond it regardless of β_{walk}. Because β_{walk} can only influence demand generated within the walkable band, and that band accounts for a structurally small share of the catchment's total distance distribution, the model's peak-hour demand output, and by extension the stress-test scenarios built upon it, is not fragile to the specific transferred value of β_{walk} adopted in Section 3.3.2.

***Table 1**. Sensitivity of Modified Gravity Model Demand Output to β_{walk}, $\beta_{transit}$ and the 400 m breakpoint held fixed.*

β_{walk}	Total Pd-weighted mass (% change vs. base)	Walkable-zone demand share	Implied peak-hour trips
1.2	+2.9%	20.0%	915
1.5	+1.4%	18.8%	901
1.8 (adopted)	— (base)	17.7%	889
2.1	−1.3%	16.6%	878

3.3.3 k-factor framework and temporal load distribution

Total daily demand is distributed into hourly arrival rates using a peak-hour factor k, defined as the proportion of daily transit demand occurring within a specific one-hour window. The simulation uses k = 0.12 for the AM peak (08:00 to 10:00), k = 0.10 for the PM peak (16:00 to 18:00), and k = 0.04 for the off-peak baseline (12:00 to 14:00). These initial k-factors are subsequently evaluated against empirical data from the existing network (Section 3.5).

3.4 Macroscopic simulation: Machinations DES architecture

3.4.1 Petri Net logic and node architecture

The Machinations model represents the station as a bipartite directed graph following Petri Net theory [20]: places (pools) represent spatial capacity nodes, and transitions (gates) represent throughput-constrained processing points. Passenger entities enter via source nodes driven by the Gravity Model arrival rates and traverse the following sequential node chain: pedestrian approach → east/west entrance gate → pre-ticketing concourse → AFC gates → Skywalk Concourse → escalators/lifts/stairs → platform → train drain. The Skywalk Concourse is modelled as a pool with a physical capacity of 400 passengers, derived from the architectural square footage of the concourse level. The platform pool capacity is 780 passengers; the AFC processing rate is 30 passengers per gate per minute (aggregate 90 passengers per minute for the three operational inbound gates). Processing times and spatial capacities are sourced from SRT Phase II planning documents and established transit engineering standards.

***Table 2**. Simulation node parameters in the Machinations model.*

Architectural component	Node type	Value	Stochastic treatment

Pedestrian arrival	Source	Variable (Gravity Model output)	Poisson
Ticketing unpaid area	Pool	2 gates	Deterministic
AFC	Gate	30 pax/gate/min	Monte Carlo
Skywalk Concourse	Pool	400 pax	Deterministic limit
Escalators	Pool	60 sec transit time	Deterministic
Lifts	Pool	10 pax capacity	Deterministic
Stairs	Pool	60 sec transit time	Deterministic
Platform	Pool	780 pax	Deterministic

3.4.2 Stochastic parameters and Monte Carlo execution

Deterministic processing rates are insufficient for stress-testing. AFC gate processing times incorporate stochastic variance (±5%) via Monte Carlo methods, simulating fare-card failures and micro-delays. Vertical circulation routing (escalator, lift, stair) is governed by randomised probability distributions. Each scenario is executed for 200 iterations; statistical convergence, assessed via a moving average of Maximum Platform Occupancy, was confirmed after 120 to 150 iterations in all cases, establishing a 95% confidence interval for the primary performance metrics.

3.5 Microscopic cross-validation: AnyLogic pedestrian simulation

Cross-validation is performed using AnyLogic's Pedestrian Library, which models passengers as autonomous agents subject to continuous-space physics: collision avoidance, velocity adjustment under density, and empirical speed-density relationships. Rather than replicating the entire station, the AnyLogic environment isolates the most critical vertical circulation bottleneck, the Skywalk Concourse to platform transition, applying identical spatial geometry, capacity constraints, and off-peak arrival rates from the Machinations model. Agreement between the two tiers is assessed via relative variance in queue accumulation and average passenger clearance time at the bottleneck node. Under the off-peak baseline, relative variances of 13.19% (Skywalk Concourse peak occupancy), 15.38% (average wait time), and 13.64% (concourse clearance time) were obtained across the three primary metrics, all within the accepted 10 to 15% cross-validation tolerance for hybrid macro-micro simulation.

3.6 Stress-test scenarios

Six scenarios are defined across three disruption categories, summarised in Table 3. SC-01 and SC-02 establish off-peak and AM peak baselines under perfect operational conditions. SC-03 degrades one inbound AFC gate (33% capacity reduction, East exit) under AM peak load; SC-04 takes the primary platform-to-concourse escalator pair offline under AM peak conditions. SC-05 introduces a 10-minute train headway delay under peak surge conditions, generating compounded platform accumulation and platooned train arrivals. SC-06 injects an impulse load of 1,500 passengers over a 20-minute post-event window through the East entrance, simulating a stadium or concert egress, at approximately 1.9 times the standard AM peak ingress volume.

Table 3. *Defined stress-test scenarios for station resilience evaluation.*

Scenario	Classification	Load condition	Simulated disruption	Primary evaluation metric
SC-01	Normal baseline	Off-peak (k=0.04)	Perfect operations	Standard clearance times
SC-02	AM peak baseline	Peak hour (k=0.12)	Perfect operations	Baseline queue accumulation
SC-03	Minor disruption	Peak hour (k=0.12)	1 AFC gate offline (East exit)	Concourse queue spillback
SC-04	Technical breakdown	Peak hour (k=0.12)	Primary escalator pair offline	Vertical transition bottleneck

SC-05	Headway platooning	Peak surge	10-minute train delay	Platform spatial limits (PLOS)
SC-06	Special event surge	Impulse load, East entrance	1,500-pax concert egress	Maximum exterior holding capacity

All scenarios are evaluated against Pedestrian Level of Service (PLOS) thresholds from the Transit Capacity and Quality of Service Manual (TCQSM), graded from LOS A (>1.2 m²/passenger, free flow) to LOS F (<0.2 m²/passenger, breakdown). The concourse spillback threshold and the 2-minute maximum wait time at any single transition node are used as complementary operational failure criteria.

***Table 4**. Pedestrian Level of Service (PLOS) thresholds for transit waiting areas (TCQSM).*

LOS	Density threshold (m²/pax)	Description	Operational status
A	> 1.2	Free circulation	Optimal
B	0.9–1.2	Minor restriction, comfortable waiting	Optimal
C	0.6–0.9	Noticeable restriction, flow maintained	Acceptable
D	0.3–0.6	Severely restricted, contact possible	Critical capacity
E	0.2–0.3	Maximum capacity, flow stutters	System stress
F	< 0.2	Breakdown, crush conditions	Failure

3.7 Empirical validation methodology

3.7.1 Dataset and proxy station selection

Because Thammasat is pre-operational, demand assumptions cannot be validated directly. Instead, a twelve-month weekday origin-destination dataset (n = 260 weekdays) was obtained from the SRT Red Line Phase I network, covering all thirteen operational stations from Taling Chan (KTW) to Rangsit (RST) at hourly resolution. Two stations were selected as behavioural proxies: Rangsit (RST, RN10), the current northern terminus and structural analogue to Thammasat's prospective line-end role; and Lak Hok (LHK, RN09), the existing university-adjacent station serving Rajamangala University of Technology Thanyaburi (RMUTT) Rangsit Campus, the closest available analogue to Thammasat's "university-adjacent, terminus-proximate" character.

3.7.2 k-factor extraction and benchmarking

For each station, AM and PM peak-hour demand shares (peak-hour entries as a percentage of daily entries), entry and exit peak-to-mean ratios, and peak hour of day are extracted from the hourly OD records. These empirical k-factors are then compared directly against the simulation's assumed k parameters (12% AM, 10% PM) to assess whether the model's temporal load assumptions are consistent with observed peaking behaviour at structurally comparable existing stations [22].

3.8 Station typology classification

3.8.1 Classification dimensions

The typology is constructed across four dimensions. The primary dimension is temporal demand shape, derived from the OD dataset: AM and PM peak-hour shares, and entry and exit peak-to-mean ratios. These shape features characterise how concentrated a station's demand is in time, independently of total volume. A second classification uses the same shape features together with average daily entry volume, enabling assessment of how overall station scale interacts with demand concentration. A third dimension characterises network role, specifically terminus, interchange, or mid-line position, derived from line topology. A fourth dimension covers

spatial and built-environment context: land-use composition, building density, and points of interest (POIs) within a 1 km radius of each station, derived from OpenStreetMap via the *osmnx* library. A fifth, qualitative dimension captures architectural typology through inspection of as-built vertical circulation drawings for the two proxy stations (escalator and lift provision, spatial arrangement along the station footprint, concourse configuration), allowing the demand-based typology to be enriched with structural context.

3.8.2 Clustering approach

K-means clustering (k = 3, determined via hierarchical clustering as an initialisation step) is applied separately to the shape-only and volume-inclusive feature sets, following the approach demonstrated for transit station classification by Pang et al. [23]. All features are standardised prior to clustering. Thammasat is positioned within the resulting typology by comparing its expected demand characteristics, inferred from the proxy station analysis, against each cluster's centroid.

3.9 Climate stress-testing methodology

3.9.1 ERA5 historical baseline

A thermal baseline for the Thammasat station area is established using ERA5 fifth-generation reanalysis data [25], sourced from the Copernicus Climate Data Store at 0.25° × 0.25° spatial resolution, covering 1990 to 2024. Monthly mean near-surface air temperature (tas), specific humidity (huss), and surface pressure (ps) are extracted for the grid cell encompassing the study area (approximately 14.0°N, 100.75°E). Relative humidity is derived from specific humidity and surface pressure using the August-Roche-Magnus approximation, and the Rothfusz Heat Index regression [24] is then applied to the resulting temperature-relative humidity pairs. ERA5 uses valid_time as its time dimension and descending latitude ordering; slice notation is adjusted accordingly.

3.9.2 CMIP6 ensemble construction

Future Heat Index trajectories are derived from three CMIP6 global climate models [26]: ACCESS-CM2, IPSL-CM6A-LR, and MPI-ESM1-2-LR, selected to span a range of climate sensitivities and model lineages. For reproducibility, the specific ensemble member and grid label used for each model are: ACCESS-CM2 (r1i1p1f1, gn), IPSL-CM6A-LR (r1i1p1f1, gr), and MPI-ESM1-2-LR (r1i1p1f1, gn), consistent across all three experiments and all three extracted variables. For each model, three experiments are used: historical (1850 to 2014), SSP2-4.5 (intermediate emissions), and SSP5-8.5 (high emissions), with outputs spliced at 2015 to produce continuous 1990 to 2050 trajectories. The three model variables (tas, huss, ps) are extracted, specific humidity converted to relative humidity, and the Rothfusz Heat Index applied with a validity mask (temperature ≥ 26.7°C, relative humidity ≥ 40%) consistent with the formula's specified operating range. A five-year rolling mean is applied to suppress inter-annual variability before ensemble construction. The ensemble mean and spread are computed across the three models under each SSP scenario.

3.9.3 Bias framing and delta-change interpretation

A persistent cold-dry bias of approximately 1.5 to 2°C in the CMIP6 ensemble relative to ERA5 is observed over the study area. This offset arises from three compounding sources: coarse spatial resolution precluding the local urban heat island, systematic overrepresentation of tropical convective mixing at GCM grid scale, and the nonlinear amplification of temperature bias by the humidity term in the Heat Index computation [27]. Rather than applying post-hoc bias correction, this study follows established practice in climate impact assessment [27] by treating ERA5 as the absolute baseline and using CMIP6 output for the direction and rate of change only, an approach denoted delta-change framing. Heat Index milestones (critical thresholds linked to reduced outdoor pedestrian tolerance) are identified on the ERA5-anchored trajectory; CMIP6 projections indicate when and at what rate those milestones are approached under each SSP. This framing is presented explicitly as a methodological transparency measure rather than a limitation to be concealed.

3.9.4 Linkage to simulation scenarios

Heat Index projections are linked to the simulation framework through the catchment-shrinkage hypothesis: as ambient Heat Index increases, the effective walking distance commuters are willing to tolerate contracts, concentrating demand from outer walkable zones toward the station entrance. This mechanism directly elevates the proportion of demand arriving in a narrow temporal window, analogous to the conditions modelled in SC-05 and SC-06. The critical window identified in the projections, approximately 2040 to 2050 under SSP5-8.5, represents the period by which Heat Index-driven catchment shrinkage is expected to materially amplify the peak-hour concentration already demonstrated to exceed station capacity thresholds in those scenarios.

4. Results

4.1 Demand baseline, cross-validation, and operational performance

This section summarises the simulation baseline that underlies the empirical and climate-driven analyses presented in subsequent sections. A modified gravity model first generated the station's peak-hour demand profile from the 13-zone catchment area. The Machinations macroscopic model was then cross-validated against the AnyLogic microscopic 3D simulation to confirm kinematic consistency, and the resulting cross-validated model was used to characterise baseline operational performance (SC-01, SC-02) and localised hardware-failure resilience (SC-03, SC-04).

4.1.1 Demand generation

Peak-hour transit demand was generated using a piecewise gravity model with distance-decay impedance (β = 1.8 for pedestrian-range trips, $d \leq 0.4$ km; $\beta = 0.5$ for vehicular-feeder trips, $d > 0.4$ km), applied stochastically across the 13 catchment zones. The aggregate peak-hour inflow used to drive all subsequent scenarios is 889 trips, with zone-by-zone contributions summarised in Table 5.

***Table 5**. Aggregated peak-hour trip generation by catchment zone (condensed).*

Zone	Walkable core (0–0.2 km)	Walkable fringe (0.2–0.4 km)	Transit/feeder (0.4–2.0 km)	Vehicle-dependent (>2.0 km)
Zone 6	200	110	0	0
Zone 10	0	0	279	0
Zones 3, 11, 13	0	0	0	214
Zones 7, 9 (others)	0	0	86	0
Total	200	110	365	214

4.1.2 Cross-validation

To confirm that the Machinations state-machine logic reproduces the spatial dynamics captured by AnyLogic's continuous-physics pedestrian engine, both models were run under the off-peak baseline (SC-01, k = 0.04) and compared on Skywalk Concourse occupancy, wait time, clearance time, and density (Table 6). AnyLogic recorded systematically higher values (13 to 15% relative difference), attributable to physical queuing friction and collision avoidance that the discrete-event Machinations model abstracts away, within the accepted cross-validation tolerance for hybrid macro-micro simulation. Both models agreed on the operationally decisive outcome, Peak Level of Service (PLOS) A, supporting Machinations as a corroborated macroscopic surrogate for the higher-iteration stress-test scenarios (SC-02 to SC-06).

***Table 6**. Computational cross-validation results, SC-01 off-peak (Machinations vs. AnyLogic).*

Performance metric	Machinations	AnyLogic	Unit	% diff

Max Skywalk Concourse occupancy (Pmc)	125	144	pax	13.2
Average wait time (twc)	11	13	sec	13.2
Concourse clearance time (Tcc)	0.38	0.44	min	13.2
Concourse density	3.34	2.90	m²/pax	15.2
Peak PLOS	A	A	—	—

4.1.3 Baseline and hardware-failure performance

With the model cross-validated, the off-peak (SC-01, k = 0.04), AM-peak (SC-02, k = 0.12), and PM-peak (SC-02, k = 0.10) scenarios establish the station's baseline operational envelope. The AM-peak alighting surge (806 pax) elevates platform occupancy to LOS B (1.13 m²/pax, 4.74 min clearance), while the Skywalk Concourse remains at LOS A throughout all baseline conditions (Table 7).

Two localised hardware-failure scenarios were then introduced under AM-peak load. SC-03 (one AFC gate offline, 33% reduction in east-exit capacity) shifts spatial accumulation from the platform to the Skywalk Concourse, which absorbs the additional queue without leaving LOS A, an early indication of the concourse's buffering capacity that is examined more directly in Section 4.2. SC-04 (primary escalator offline, flow rerouted to stairwells) is markedly more severe: platform occupancy rises to 1,407 pax, clearance time nearly doubles to 8.28 min, and platform LOS degrades to C, with a secondary bottleneck pushing the concourse to LOS B. Even under this degraded condition, the platform clears within the 20-minute train headway, indicating structural viability without cascading multi-train failure. The full comparative KPI set is given in Table 7.

***Table** 7. Comparative key performance indicators across baseline (SC-01, SC-02) and hardware-failure (SC-03, SC-04) scenarios.*

Performance Metric	SC-01 (k=0.04)	SC-02 AM (k=0.12)	SC-02 PM (k=0.10)	SC-03 AFC Fail	SC-04 ESC Fail	Unit
Platform						
Max occupancy (Pmp)	274	806	693	820	1407	pax
Avg wait time (twp)	48	142	122	145	248	sec
Clearance time (Tcp)	1.61	4.74	4.08	4.82	8.28	min
Density	3.32	1.13	1.31	1.11	0.65	m²/pax
PLOS	A	B	A	B	C	—
Skywalk Concourse						
Max occupancy (Pmc)	125	154	147	147	446	pax
Avg wait time (twc)	11	14	13	13	41	sec
Clearance time (Tcc)	0.38	0.47	0.45	0.45	1.35	min
Density	3.34	2.71	2.84	2.84	0.94	m²/pax
PLOS	A	A	A	A	B	—

Together, these results establish a demand baseline of 889 peak-hour trips, a cross-validated simulation model, and an operational envelope in which the Skywalk Concourse consistently absorbs spatial accumulation before it reaches the platform, a pattern examined under more severe conditions in Section 4.2.

4.2 Network disruption and impulse-load resilience: the Skywalk Concourse as a passive crowd buffer

Section 4.1 established that the station performs within acceptable Level of Service (LOS) bounds under nominal peak loading and localised hardware failures, with the Skywalk Concourse consistently outperforming the platform. This section extends that analysis to two more severe stress conditions: a system-level rail network delay (SC-05, platform platooning) and an extreme exogenous impulse load (SC-06, stadium event egress). Together, these scenarios reveal the station's most significant architectural property, namely the capacity of the Skywalk Concourse to function as a passive spatial buffer that absorbs crowd pressure before it can compromise the platform.

4.2.1 SC-05: platform platooning under network delay

SC-05 simulates a 10-minute headway compression caused by an upstream rail delay: a train scheduled for minute 40 arrives at minute 50, immediately followed by the on-time minute-60 service. This compresses two alighting batches (approximately 800 pax in total) into a 10-minute window, against a combined vertical-circulation processing capacity of 170 pax/min.

The compressed arrival produces a residual platform queue at the second train's arrival, raising maximum platform occupancy to 835 pax (versus 806 pax at baseline AM-peak), with clearance time increasing marginally to 4.91 min and platform LOS remaining at B (Table 8). Critically, the Skywalk Concourse is almost entirely insulated from this disruption: its maximum occupancy (151 pax), clearance time (0.46 min), and PLOS (A) are statistically indistinguishable from the undisturbed AM-peak baseline (154 pax, 0.47 min, A). The vertical-circulation hardware absorbs the platooning shock at the platform-concourse interface, preventing it from propagating upward.

This result indicates that the station’s vertical circulation capacity is over-engineered relative to railway-induced headway disruptions of this magnitude: even back-to-back platooned trains do not generate a compounding queue.

4.2.2 SC-06: stadium event impulse load

SC-06 simulates the egress phase of a major event at the adjacent stadium complex: a 1,500-passenger impulse load, modelled as 75 pax/min arriving at the east (university-side) entrance over a concentrated 20-minute window, an arrival rate that substantially exceeds the station's downward processing capacity. This volume was established as a conservative assumption representing a concentrated, fractional egress from the university's stadium and event facilities: assuming a standard regional stadium capacity, the 1,500-passenger figure corresponds to approximately 10% of total attendees choosing rail transit and arriving at the station boundary simultaneously within the post-event window, rather than an arbitrary or worst-case total.

Under this load, the Skywalk Concourse transforms from a transient pass-through space into a high-density holding area, with maximum occupancy reaching 415 pax, nearly three times the AM-peak baseline (154 pax), while maintaining a density of 1.01 m²/pax and PLOS B (Table 8). Because the vertical-circulation hardware and AFC gates meter the downward flow at a rate the platform can safely absorb, platform occupancy rises only modestly to 865 pax (versus 806 pax at baseline), remaining at PLOS B with a density of 1.05 m²/pax.

The mechanism is structurally identical to, but far more pronounced than, the SC-03 result in Section 4.1: a downstream capacity constraint causes an upstream spatial accumulation, and the station’s architecture, specifically the unhindered width of the Skywalk Concourse, absorbs that accumulation at a safe density.

***Table 8**. Platform and Skywalk Concourse performance under network-delay (SC-05) and impulse-load (SC-06) conditions, with AM-peak (SC-02) as reference.*

Performance Metric	SC-05 Platooning	SC-06 Stadium Surge	SC-02 reference	Unit
Platform				
Max occupancy (Pmp)	835	865	806	pax

Avg wait time (twp)	147	153	142	sec
Clearance time (Tcp)	4.91	5.09	4.74	min
Density	1.09	1.05	1.13	m²/pax
PLOS	B	B	B	—
Skywalk Concourse				
Max occupancy (Pmc)	151	415	154	pax
Avg wait time (twc)	14	38	14	sec
Clearance time (Tcc)	0.46	1.26	0.47	min
Density	2.76	1.01	2.71	m²/pax
PLOS	A	B	A	—

4.2.3 Synthesis: spatial metering as a system property

Table 9 consolidates key performance indicators across all six simulated scenarios. Two patterns emerge consistently. First, platform performance degrades gracefully under all tested disruptions except SC-04 (escalator failure with stair rerouting), which is the only scenario to reach platform LOS C; even then, clearance occurs within the 20-minute train headway. Second, and more significantly, Skywalk Concourse occupancy scales with the severity of downstream or downstream-adjacent disruption, from 125 pax (SC-01) to 446 pax (SC-04) and 415 pax (SC-06), while never exceeding PLOS B.

***Table 9**. Comparative key performance indicators across all six simulated scenarios (SC-01 to SC-06).*

Scenario	Condition	Max Platform (Pmp)	Platform Clear. (Tcp)	Platform PLOS	Max Skywalk (Pmc)	Skywalk PLOS
SC-01	Baseline Off-Peak (k=0.04)	274	1.61 min	A	125	A
SC-02	Baseline AM Peak (k=0.12)	806	4.74 min	B	154	A
SC-03	AFC Gate Failure (33% loss)	820	4.82 min	B	147	A
SC-04	Escalator Failure (stair routing)	1407	8.28 min	C	446	B
SC-05	Network Platooning (10-min gap)	835	4.91 min	B	151	A
SC-06	Stadium Impulse Load (1,500 pax)	865	5.09 min	B	415	B

This pattern indicates that the hardware constraints which might conventionally be read as design bottlenecks, namely escalator and AFC gate capacities, instead function as a passive crowd-metering system. By throttling downward flow to a rate the platform can safely absorb, these constraints route spatial stress into the Skywalk Concourse, whose architectural width provides sufficient buffer capacity to hold the resulting accumulation at LOS A to B across every tested scenario, including an exogenous impulse load equivalent to roughly 1.9 times the AM-peak design volume. This passive-buffer behaviour, emerging from the interaction between vertical-circulation capacity and concourse geometry rather than from any active crowd-management intervention, is the station's most significant architectural property and forms the basis for the climate-adaptation and typology discussions in subsequent sections.

4.2.4 Sensitivity to empirically observed k-factors

The stress-test scenarios in Sections 4.1 and 4.2 were executed using the Machinations model's assumed peak-hour k-factor (12% AM), which Section 4.3 shows to be conservative relative to all thirteen currently operating Red Line stations. This section presents an analytical sensitivity estimate of SC-06 under the empirically observed k-factor range (15 to 20% AM), to test whether the Skywalk Concourse's buffering capacity remains intact under realistic peak demand. A full stochastic re-simulation is identified as a priority for future work (Section 5.6).

Method. The SC-06 outcome is decomposed into a background AM-peak component (scaling approximately linearly with k) and a fixed impulse-load component (1,500 pax over 20 minutes, exogenous to k). The background component is re-scaled to the target k-factor, the fixed impulse contribution re-added, and the resulting occupancies converted to density using the spatial areas implied by the SC-02 baseline density figures, then graded against the PLOS thresholds in Table 3.

Result. Table 10 presents the scaled estimates. At the lower empirical bound (15% AM), the Skywalk Concourse remains at PLOS B (454 pax, 0.92 m²/pax), consistent with the buffering behaviour reported under the assumed k-factor. At the upper empirical bound (20% AM), the concourse degrades to PLOS C (518 pax, 0.81 m²/pax), the first condition examined in this study under which the concourse's buffering capacity is not maintained at PLOS B or better. The platform degrades to PLOS C at both bounds (1,066 and 1,402 pax respectively), more severe than the PLOS B reported for SC-06 under the assumed k-factor, and approaching the severity of the SC-04 escalator-failure result, the only other PLOS C outcome in this study.

***Table 10**. Analytically scaled SC-06 performance under empirical k-factor bounds, compared with the reported result under the assumed k-factor.*

Condition	Platform occupancy (pax)	Platform density (m²/pax)	Platform PLOS	Concourse occupancy (pax)	Concourse density (m²/pax)	Concourse PLOS
SC-06 reported (k=0.12)	865	1.05	B	415	1.01	B
SC-06 scaled (k=0.15)	1066	0.85	C	454	0.92	B
SC-06 scaled (k=0.20)	1402	0.65	C	518	0.81	C

Limitations. This analytical scaling is offered as an interim sensitivity check, not a re-simulation, and should be read with two important caveats. First, the linear scaling assumption does not capture non-linear queueing effects: a higher background demand could saturate AFC gates or escalators before the impulse load even arrives, producing worse outcomes than a simple proportional scale-up suggests. Second, the estimate does not capture Monte Carlo stochastic variance, since it scales single deterministic baseline figures rather than re-running the underlying stochastic processes. A full re-simulation under empirically calibrated k-factors remains a priority for future work (Section 5.6).

Despite these caveats, the direction and approximate magnitude of the result are unlikely to be artefacts of the scaling method alone: both the platform and, at the upper bound, the Skywalk Concourse show genuine PLOS degradation under realistic peak-hour demand, indicating that the passive-buffering finding in Section 4.2, while robust under the conditions originally tested, has identifiable limits that should inform any operational reliance on this mechanism.

4.3 Empirical validation of peak-hour demand assumptions

Sections 4.1 and 4.2 characterised station performance under the Machinations Gravity Model's temporal demand assumptions, including its single global “peak percentage” parameter (k = 0.12 AM, k = 0.10 PM). Because the Thammasat station is not yet operational, no direct AFC data exists for the subject site. To validate these assumptions, hourly origin-destination (OD) data from the thirteen currently operating Red Line Phase I stations (Taling Chan to Rangsit, June 2025 to May 2026) were obtained from the State Railway of Thailand and used as behavioural proxies. After cleaning, which involved reconciling archive formats, removing one degenerate zero-duration record (a single station-pair-hour entry with identical entry and exit timestamps, most likely a system logging artefact rather than a genuine trip), and verifying entry/exit totals, the dataset comprised 1,234,038 station-pair-hour records with zero checksum discrepancies. One anomaly, an extended New Year's Eve service day, was retained and documented.

Two stations were selected as proxies for the Thammasat archetype: Rangsit (RST), the current northern terminus and structural analogue to Thammasat's prospective line-end role, and Lak Hok (LHK), the existing university-adjacent station serving RMUTT Rangsit Campus and the closest available analogue to Thammasat's "university-adjacent, terminus-proximate" character.

4.3.1 Empirical demand profiles and network-wide peaking

Hourly entry and exit volumes at Rangsit, aggregated across the study year and normalised to an average weekday (n = 260) and weekend (n = 105) day, exhibit the temporal signature of a residential terminus: a pronounced single-hour morning entry peak (outbound commuting) and a broader afternoon/evening exit peak (return commuting). On weekdays, the morning entry peak occurs at 07:00 (788 pax/day, 20.3% of daily entries; entry peak-to-mean ratio 4.05), and the afternoon exit peak at 18:00 (635 pax/day, 15.3% of daily exits; ratio 3.05). The weekend profile is markedly flatter, building gradually to a broad peak around 17:00 (peak-to-mean ratios 1.52 entry / 1.82 exit), consistent with discretionary rather than commute-driven travel.

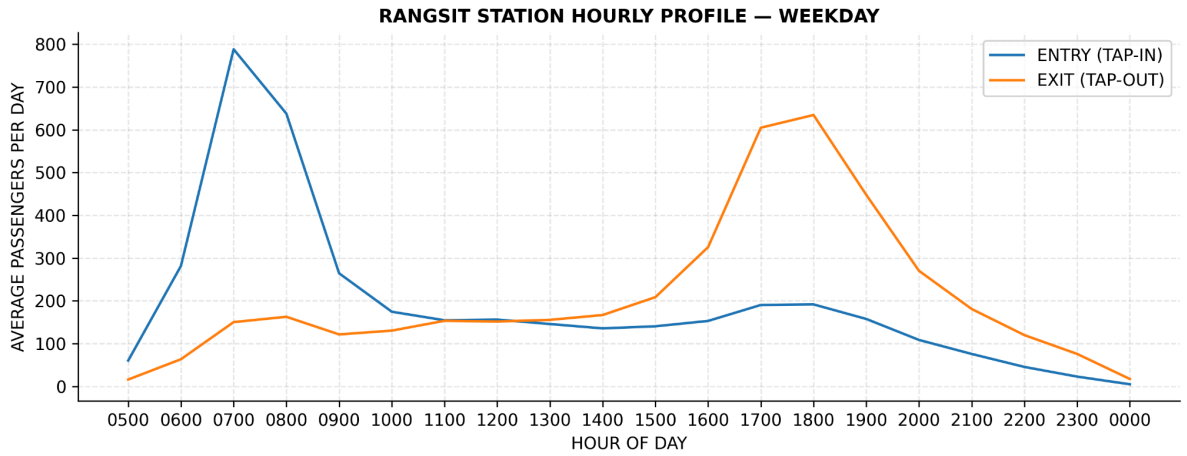

***Figure 4**. Rangsit station hourly passenger profile — weekday (average passengers per hour, 05:00–00:00).*

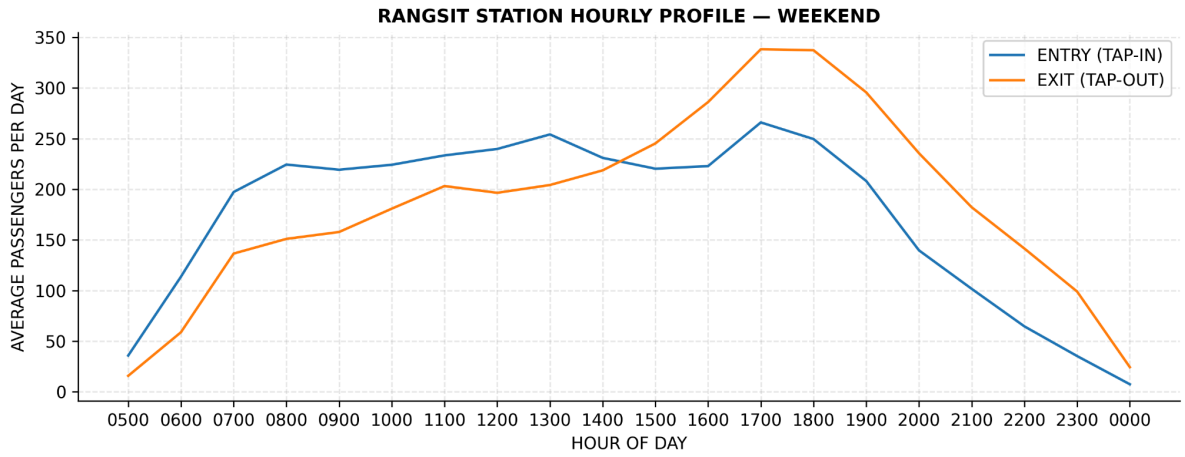

***Figure 5**. Rangsit station hourly passenger profile — weekend (average passengers per hour, 05:00–00:00).*

To assess whether this peaking behaviour is representative or exceptional, the same metrics were computed for all thirteen Phase I stations on a weekday basis (Table 11). Pronounced single-hour peaking proves to be a network-wide characteristic rather than a Rangsit-specific feature. Rangsit exhibits the highest entry peak-to-mean ratio (4.46) of the thirteen stations, consistent with its terminus role, where all outbound morning demand originates within a narrow window.

***Table 11**. Weekday hourly demand metrics for the thirteen SRT Red Line Phase I stations (average values per weekday, n = 260 days; ordered by line sequence, Taling Chan to Rangsit). Thammasat proxy stations (RST, LHK) shown in bold.*

Station	Avg. Daily Entries	Avg. Daily Exits	AM Peak Hr	AM Peak %	PM Peak Hr	PM Peak %	Entry P/M	Exit P/M
Taling Chan (RW04)	992.4	998.7	07:00	17.1	17:00	14.8	3.76	3.26
Bang Bamru (RW03)	607.7	641.6	07:00	16.8	17:00	14.6	3.69	3.22
Bang Son (RW02)	496.8	536.8	08:00	14.9	17:00	14.9	3.28	3.28
Krung Thep Aphiwat (RN01/RW01)	8321.2	8902.9	18:00	13.2	07:00	13.8	2.90	3.05
Chatuchak (RN02)	585.5	703.0	17:00	14.5	08:00	11.5	3.20	2.53
Wat Samian Nari (RN03)	1,019.2	1001.7	17:00	20.0	07:00	19.6	4.39	4.31
Bang Khen (RN04)	1877.7	1824.2	17:00	19.9	08:00	21.7	4.39	4.77
Thung Song Hong (RN05)	624.6	632.8	18:00	18.8	08:00	16.7	4.13	3.68
Lak Si (RN06)	3766.6	3866.0	17:00	13.1	07:00	11.6	2.88	2.54
Kan Kheha (RN07)	776.7	750.0	07:00	21.0	17:00	17.1	4.62	3.77
Don Mueang (RN08)	6038.1	5110.4	07:00	8.9	17:00	11.5	1.96	2.53
Lak Hok (RN09)	**1789.3**	**1659.8**	**07:00**	**15.1**	**18:00**	**12.5**	**3.32**	**2.76**
Rangsit (RN10)	**3891.2**	**4159.0**	**07:00**	**20.3**	**18:00**	**15.3**	**4.46**	**3.36**

4.3.2 Comparison with Machinations model assumptions

The Machinations Gravity Model implements temporal demand variation through a single global peak-percentage parameter (k), scaling gravity-model outputs uniformly across all thirteen catchment zones, with k = 0.04 (off-peak, SC-01), k = 0.12 (AM peak, SC-02 and derivatives), and k = 0.10 (PM peak).

Inspection of the model architecture confirmed that no finer temporal resolution exists: k is applied identically across all zones regardless of station type.

Table 12 compares these assumed k-factors against the empirically observed peak shares at the two proxy stations. At both, the empirical peak-hour demand share exceeds the corresponding k-factor: at Rangsit, the AM share (20.3%) is approximately 1.7 times the assumed k (12%), and the PM share (15.3%) approximately 1.5 times the assumed k (10%); at Lak Hok, the more directly comparable archetype for Thammasat, the corresponding ratios are 1.26 and 1.25. As Table 12 shows, this is not confined to the two proxies: all thirteen Phase I stations exhibit an AM and/or PM peak share exceeding the respective k-factor, indicating a network-wide characteristic rather than a station-specific anomaly.

***Table 12**. Comparison of Machinations Gravity Model peak-hour k-factors with empirically observed peak-hour demand shares at Rangsit (RST) and Lak Hok (LHK).*

Period	Machinations k-factor (%)	Empirical peak share — RST (%)	Empirical peak share — LHK (%)
Morning peak (AM)	12.0	20.3	15.1
Evening peak (PM)	10.0	15.3	12.5

4.3.3 Implications for the stress-test scenarios

These findings carry three implications. First, the consistent under-estimation of single-hour peak concentration suggests that the demand inputs to SC-02 and its concentrated-demand derivatives, SC-05 and SC-06, may represent conservative lower-bound estimates of peak-hour loading at Thammasat. If actual demand concentration approaches the Lak Hok (15.1% AM / 12.5% PM) or Rangsit (20.3% AM / 15.3% PM) levels rather than the assumed 12%/10%, the operational stresses identified under SC-05 and SC-06, including the conditions under which the Skywalk Concourse was found to function as a passive crowd buffer (Section 4.2), could occur at correspondingly higher intensities than simulated.

Second, the model's single global k-factor does not accommodate the station-to-station variation in peaking behaviour evident in Table 12 (entry peak-to-mean ratios ranging from 1.96 to 4.62). The materiality of this simplification depends on which station archetype Thammasat most closely resembles, an issue addressed in the typology analysis of Section 4.4. A zone- or archetype-specific k-factor, calibrated against operational data of this kind, would be a methodologically defensible refinement for future model iterations.

Third, because Thammasat is not yet operational, this validation is necessarily proxy-based: Rangsit and Lak Hok individually represent the terminus and university-adjacent generator conditions respectively, but neither replicates the combined "university-adjacent, terminus-proximate" archetype that Thammasat will embody, a limitation revisited in the Discussion.

On this basis, an empirically grounded k-factor range of approximately 15 to 20% for the morning peak and 12 to 15% for the evening peak, bracketed by the Lak Hok and Rangsit observations, is recommended as a sensitivity bound for future re-evaluation of SC-02, SC-05, and SC-06, in place of the current single-point assumptions of 12% and 10%.

4.4 Station typology and archetype classification

This section addresses Direction B of the journal expansion: the formal classification of SRT Red Line Phase I stations into demand-based archetypes, and the positioning of the prospective Thammasat University station (RN11) within this typology. The classification draws on the same twelve-month origin-destination dataset described in Section 4.3, using the weekday demand-shape metrics already established (AM and PM peak shares, and entry/exit peak-to-mean ratios) as classification features.

This typology is extended in two further dimensions: an architectural comparison of vertical circulation and concourse configuration for the two Thammasat proxy stations (Section 4.4.5), and an analysis of spatial catchment characteristics, namely land-use composition, building density, and points of interest within a 1 km radius, for all thirteen stations (Section 4.4.6).

4.4.1 Classification approach

Two complementary clustering analyses were performed using k-means clustering (k = 3) on standardised weekday demand metrics for the thirteen Red Line Phase I stations. The first analysis ("volume-inclusive") used five features: AM peak share, PM peak share, entry peak-to-mean ratio, exit peak-to-mean ratio, and average daily entry volume. The second analysis ("shape-only") used the same four peaking metrics but excluded total demand volume, isolating the temporal shape of demand from its absolute scale. Principal component analysis was not applied, as the feature set was already low-dimensional (four to five features) and the retained features carry direct physical interpretation relevant to operational planning.

With only thirteen stations available on the existing network, this typology should be read as exploratory rather than as a statistically robust classification: a three-cluster k-means solution over thirteen points yields clusters as small as three stations (Cluster 1, Section 4.4.2), and the specific cluster assignments, while consistent with each station's known network role and land use, are sensitive to the particular feature set and station sample used and should not be interpreted as a definitive or final archetype scheme for the network. The typology is best understood as a structured, descriptive lens for positioning Thammasat relative to its closest available proxies, RST and LHK, rather than as a validated classification system, a distinction maintained throughout the discussion of its implications in Sections 4.4.3 and 5.2.

The shape-only analysis is adopted as the primary typology for this section, as it isolates the temporal demand behaviour most directly relevant to evaluating the Machinations model's peak-hour assumptions (Section 4.3.2) and is more readily transferable to a new station, such as Thammasat, whose absolute demand volume is not yet known but whose demand shape can reasonably be expected to resemble that of structurally analogous existing stations. The volume-inclusive analysis is retained as a secondary, contextual classification reflecting overall station scale and network role.

4.4.2 Demand-shape typology results

The shape-only clustering produced three groups, summarised in Table 13 and illustrated in Figure 6. Cluster 0 ("Directional / Terminus-like") comprises Taling Chan (TLC), Bang Bamru (BMR), Thung Song Hong (TSH), and Rangsit (RST), characterised by high AM peak shares (17 to 20%) and high entry peak-to-mean ratios (3.7 to 4.5), indicating strongly directional, single-hour-dominated morning demand. Cluster 1 ("Sharp Peaking") comprises Wat Samian Nari (WSN), Bang Khen (BKH), and Kan Kheha (KHA), exhibiting the most extreme peaking observed on the network (AM peak shares of 20 to 21%, entry peak-to-mean ratios of 4.3 to 4.6). Cluster 2 ("Balanced / Interchange-like") comprises Krung Thep Aphiwat (KTW), Lak Si (LAK), Chatuchak (CTK), Bang Son (BSN), Lak Hok (LHK), and Don Mueang (DMG), characterised by comparatively lower AM peak shares (9 to 15%) and lower entry peak-to-mean ratios (2.0 to 3.3), consistent with demand that is more evenly distributed across the operating day.

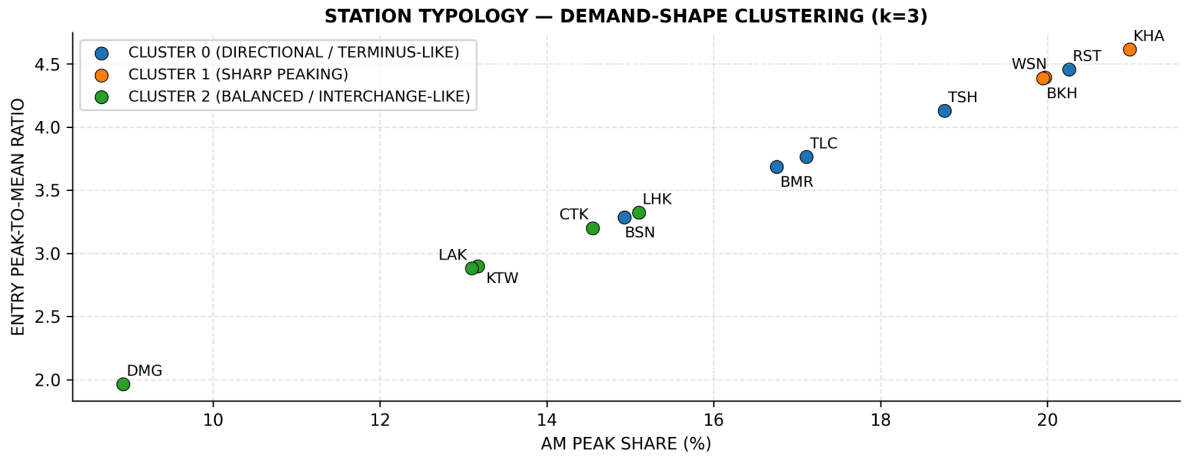

***Figure 6**. Station typology based on demand-shape clustering (k = 3): AM peak share versus entry peak-to-mean ratio for all thirteen SRT Red Line Phase I stations. Marker colour denotes cluster assignment.*

***Table 13**. Demand-shape typology of SRT Red Line Phase I stations (k-means clustering, k = 3, shape-only features).*

Cluster	Descriptive Label	Stations	Network Role Tendency
0	Directional / Terminus-like	TLC, BMR, TSH, RST	Termini and single-direction-dominant suburban stations
1	Sharp Peaking	WSN, BKH, KHA	Residential suburban stations with concentrated commute demand
2	Balanced / Interchange-like	KTW, LAK, CTK, BSN, LHK, DMG	Interchange hubs, specialised generators, and mid-line stations

4.4.3 Positioning Thammasat within the typology

A notable result of this classification is that Rangsit (RST) and Lak Hok (LHK), the two stations identified in Section 4.3 as the closest available behavioural proxies for Thammasat on the basis of network position and adjacent land use respectively, fall into different demand-shape clusters. RST is assigned to Cluster 0 (Directional / Terminus-like), while LHK is assigned to Cluster 2 (Balanced / Interchange-like). This indicates that, within the thirteen-station network, "university-adjacent" land use is not associated with a single, distinct demand-shape archetype. Rather, a station's position in the network, specifically whether it functions as a line terminus or a mid-line station, appears to be the dominant determinant of temporal demand concentration.

This finding has a direct implication for the prospective Thammasat station. Under the Phase II extension, Thammasat will become the new northern terminus of the Red Line, with Rangsit transitioning from terminus to a mid-line, through-station role. If network position is indeed the dominant driver of demand shape, as the clustering results suggest, then Thammasat may be expected to inherit a demand profile resembling RST's current Cluster 0 (Directional / Terminus-like) profile, characterised by a pronounced single-hour morning peak (AM peak share approximately 17 to 20% of daily entries, entry peak-to-mean ratio approximately 3.7 to 4.5), rather than LHK's more moderate, balanced Cluster 2 profile. This is consistent with, and provides a structural explanation for, the empirical k-factor comparison in Section 4.3.2, in which RST's observed peak shares (20.3% AM / 15.3% PM) exceeded the Machinations model's assumed k-factors (12% AM / 10% PM) by a wider margin than LHK's (15.1% AM / 12.5% PM).

On this basis, Thammasat is provisionally classified as belonging to the “Directional / Terminus-like” archetype (Cluster 0), with the caveat that the magnitude of its university-generated demand component, absent from RST's current catchment but present at LHK, may shift its profile somewhat toward Cluster 2 relative to a pure terminus station. A provisional composite characterisation of Thammasat as a "university-adjacent,

terminus-proximate" archetype, combining the terminus-driven peaking of Cluster 0 with a secondary, partially offsetting moderation effect from university-generated demand as observed at LHK, is therefore recommended as the working hypothesis for SC-02, SC-05, and SC-06 scenario refinement.

4.4.4 Volume-inclusive classification and future enrichment

For completeness, a second clustering analysis was performed using k-means (k = 3) on the same four shape metrics together with average daily entry volume as a fifth feature, with all features standardised prior to clustering. The resulting volume-inclusive typology is reported in Table 14.

This classification separates the three highest-volume stations, Krung Thep Aphiwat (KTW), Lak Si (LAK), and Don Mueang (DMG), from the remaining ten stations. These three stations form Cluster 2 ("High-volume hub, flat profile"), with mean daily entries of approximately 6,042, an order of magnitude above the other two clusters, but the flattest demand profile of the three (AM peak share 11.7%, entry peak-to-mean ratio 2.58, both the lowest values observed), consistent with their role as interchange and specialised-access hubs serving demand distributed across the operating day.

The remaining ten stations split into Cluster 0 ("Low-volume, moderate peaking": TLC, BMR, BSN, CTK, LHK; mean daily entries approximately 894, AM peak share 15.7%, entry peak-to-mean ratio 3.45) and Cluster 1 ("Moderate-volume, sharp peaking": WSN, BKH, TSH, KHA, RST; mean daily entries approximately 1,638, AM peak share 20.0%, entry peak-to-mean ratio 4.40, the sharpest peaking of all three clusters).

Table 14. *Volume-inclusive typology of SRT Red Line Phase I stations (k-means clustering, k = 3, including average daily entry volume).*

Cluster	Descriptive label	Stations	Network role tendency
0	Low-volume, moderate peaking	TLC, BMR, BSN, CTK, LHK	Lower-demand suburban and university-adjacent stations with moderate directional peaking
1	Moderate-volume, sharp peaking	WSN, BKH, TSH, KHA, RST	Residential and terminus stations with the most concentrated commute-driven demand
2	High-volume hub, flat profile	KTW, LAK, DMG	Interchange and specialised-access hubs with high overall volume but evenly distributed demand across the day

Notably, when volume is introduced as a classification feature, both Thammasat proxy stations move to different clusters than those identified in the shape-only typology (Section 4.4.2, Table 13). Rangsit (RST), assigned to Cluster 0 ("Directional/Terminus-like") in the shape-only typology, joins Cluster 1 ("Moderate-volume, sharp peaking") here. Lak Hok (LHK), assigned to Cluster 2 ("Balanced/Interchange-like") in the shape-only typology, joins Cluster 0 ("Low-volume, moderate peaking") here.

This indicates that the two classifications are not simply complementary views of the same underlying grouping, in which volume would add a secondary axis on top of an otherwise stable shape-based structure. Rather, incorporating volume substantially reshuffles the typology for the two stations most relevant to Thammasat. Both proxies move into lower-volume clusters than KTW, LAK, and DMG, which is unsurprising given their position in the network, but the direction of their relative movement is informative: RST moves toward the cluster with the sharpest peaking behaviour of the entire network, while LHK moves toward a cluster with more moderate peaking. This suggests that RST's terminus status and LHK's university-adjacency may interact differently with overall demand volume, a distinction that the shape-only typology, by construction, cannot capture.

For the Thammasat application, this introduces a further open question alongside those raised in Section 4.4.3 and Section 4.4.5. If Thammasat's eventual demand volume more closely resembles RST's, the volume-inclusive typology would place it among the sharpest-peaking stations on the network, reinforcing the

"Directional/Terminus-like" working hypothesis from Section 4.4.3. If its volume instead resembles LHK's, the same typology would place it in the more moderate Cluster 0, partially offsetting that hypothesis. Resolving this will depend on demand volume estimates for Thammasat that are not yet available, and is revisited in the Discussion (Section 5).

The typology presented here is based exclusively on operational demand data and is therefore behavioural rather than spatial or architectural in nature. Two further dimensions extend this typology in the remainder of this section: an architectural comparison of vertical circulation and concourse configuration (Section 4.4.5), and an analysis of spatial catchment characteristics derived from OpenStreetMap, namely land-use composition, building density, and points of interest within a 1 km radius of each station (Section 4.4.6).

4.4.5 Architectural enrichment: vertical circulation and concourse configuration

Sections 4.4.1 to 4.4.4 established a typology of station archetypes derived from operational demand shape, in which Rangsit (RST) and Lak Hok (LHK), the two Thammasat proxy stations identified in Section 4.3, were assigned to different clusters (Cluster 0, "Directional/Terminus-like", and Cluster 2, "Balanced/Interchange-like", respectively). This section examines whether the as-built architectural configuration of these two stations is consistent with, and offers additional explanatory depth to, that demand-based classification. As-built reference plans for vertical circulation (escalators and lifts) at concourse and platform levels were inspected for both stations, together with a generic "typical station" reference plan used as a structural baseline across the line.

Vertical circulation capacity

The typical station reference plan specifies a baseline vertical circulation provision of four escalators and two lifts per level transition (ground-to-concourse and concourse-to-platform), totalling eight escalators and four lifts across both transitions. Against this baseline, RST is provisioned with twelve escalators (ESC.01 to ESC.12) and six lifts (L.01 to L.06) across the two level transitions, approximately 1.5 times the typical allocation. LHK, by contrast, is provisioned with six escalators (ESCALATOR-03 to -06, plus two units recorded as omitted) and two lifts (ELEVATOR-01/02) at concourse level, below the typical allocation for a single level transition.

This differential is consistent with the demand-based typology: RST's elevated vertical circulation capacity corresponds to its classification as a high-volume, directional/terminus-like station (Cluster 0), while LHK's comparatively modest provision, further reduced by the omission of two escalator units referenced against drawing CSC/CC2/CS.711533, is consistent with its classification as a lower-volume, balanced-flow station (Cluster 2).

Spatial distribution of access points

Beyond simple counts, the spatial arrangement of vertical circulation elements reveals a more substantive architectural distinction between the two stations. At RST, escalators and lifts are distributed across the full length of the station footprint (approximately 300 m, spanning structural grid lines 0 to 10) at both the ground-to-concourse and concourse-to-platform transitions. Figure 7 (concourse-to-platform) shows this distributed arrangement: vertical circulation elements recur at six distinct positions along the concourse, grid lines 1, 2, 3, 5, 7, and 9 to 10, rather than converging on a single entrance or transfer point. Figure 8 (ground-to-concourse) shows the same general distributed pattern but with fewer elements overall, retaining activity at grid lines 1, 3, 5, and 9 to 10 while omitting the grid 2 and grid 7 elements present at the concourse-to-platform level. This indicates that RST functions as a multi-node access station along its length, with several parallel pedestrian streams distributing across the platform independently, though provision is somewhat reduced at the ground-to-concourse transition relative to the concourse-to-platform transition above it.

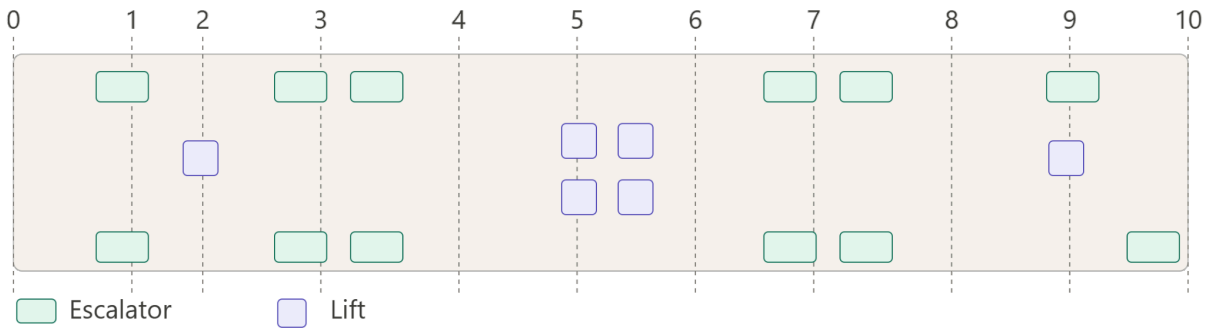

***Figure 7**. Schematic representation of vertical circulation arrangement at Rangsit (RST) station, concourse-to-platform level. The diagram is a manually redrawn simplification of the as-built reference plan, showing the station footprint (approximately 298 m, grid lines 0 to 10) and the approximate position of each escalator and lift; it is not to scale and omits structural and architectural detail present in the original drawing. The full as-built reference plan is provided in Supplementary Material (source: drawing CC2-ABMW-S903-17.0001.00).*

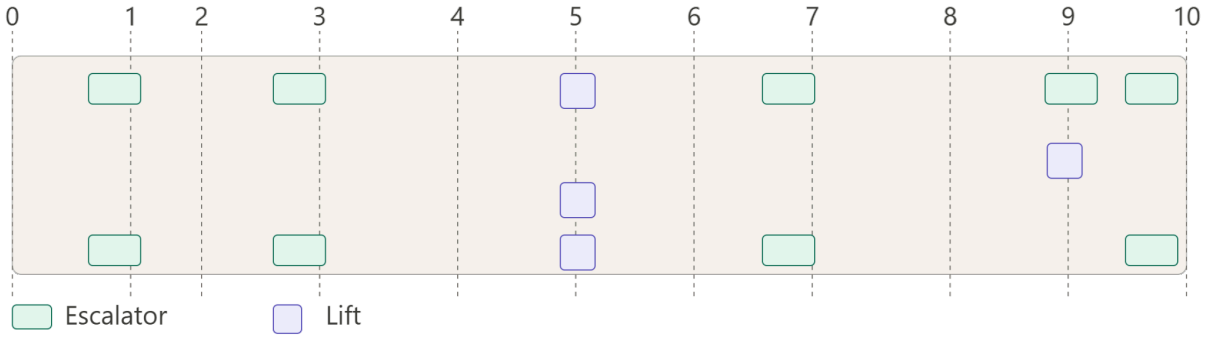

***Figure 8**. Schematic representation of vertical circulation arrangement at Rangsit (RST) station, ground-to-concourse level. As with Figure 7, this is a manually redrawn simplification of the as-built reference plan, retaining the same footprint and grid lines (0 to 10) for direct comparison, and showing the approximate position of each escalator and lift; note the reduced element count relative to Figure 7 (Section 4.4.5). It is not to scale and omits structural and architectural detail present in the original drawing. The full as-built reference plan is provided in Supplementary Material (source: drawing CC2-ABMW-S902-17.0001.00).*

LHK presents a markedly different spatial signature (Figure 9). Within its shorter footprint (approximately 240 m, grid lines 1 to 9), vertical circulation is concentrated into two discrete clusters located toward the western half of the concourse: an escalator pair near grid line 2 (ESCALATOR-03/04) and a combined escalator and lift cluster spanning grid lines 4 to 6, with a lift pair at grid line 4 (ELEVATOR-01/02) and an escalator pair at grid line 6 (ESCALATOR-05/06). The eastern half of the concourse, grid lines 7 to 9, is unequipped. The two escalator units recorded as omitted are located at the extreme western and eastern ends of the concourse (grid lines 0 and 9), asymmetrically bookending the two active clusters.

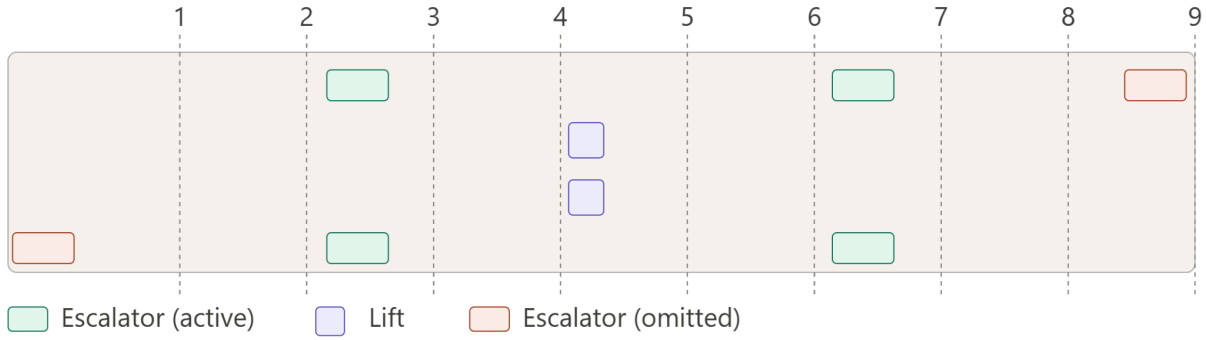

***Figure 9**. Schematic representation of vertical circulation arrangement at Lak Hok (LHK) station, concourse level. The diagram is a manually redrawn simplification of the as-built reference plan, showing the station footprint (approximately 240 m, grid lines 1 to 9), the two active escalator and lift clusters near grid lines 2 and 4 to 6, the unequipped eastern section (grid lines 7 to 9), and the two omitted escalator units at grid lines 0 and 9 (Ref. CSC/CC2/CS.711533); it is not to scale and omits structural and architectural detail present in the original drawing. The full as-built reference plan is provided in Supplementary Material (source: drawing CC2-ABMW-S803-17.0001.00)*

Implications for the typology and the Thammasat application

The architectural evidence reinforces the demand-based separation of RST and LHK into different clusters, but it also adds a dimension that the demand-shape features alone (AM/PM peak share, entry/exit peak-to-mean ratios) do not capture: the spatial topology of access. RST's distributed, multi-node configuration and LHK's bookended, two-cluster configuration represent qualitatively different pedestrian circulation strategies, not merely different scales of the same strategy. This suggests that station architecture may constitute an independent classification axis, orthogonal to demand shape, that could refine the typology in future work, for example by distinguishing "distributed-access" from "node-access" station designs within a given demand cluster.

For the Thammasat station application, the implications of this distributed versus concentrated access pattern are discussed in Section 5.3, pending architectural drawings from the SRT data request. Architectural provision should be read as an upper bound on intended capacity, not a direct proxy for current observed demand.

***Table 15**. Comparison of vertical circulation provision and spatial topology, typical station baseline versus RST and LHK.*

Characteristic	Typical station	RST (Cluster 0)	LHK (Cluster 2)
Total escalators	8 (4 per transition)	12	6 (2 omitted)
Total lifts	4 (2 per transition)	6	2
Concourse footprint	n/a	approximately 300 m (grid 0 to 10)	approximately 240 m (grid 1 to 9)
Access topology	n/a	Distributed, multi-node (3 to 4 clusters along full length)	Concentrated, two-cluster (bookended, open centre)

4.4.6 Spatial catchment characteristics

To complement the behavioural and architectural dimensions above, land-use composition, building density, and point-of-interest (POI) counts within a 1 km radius of each station were extracted from OpenStreetMap using the *osmnx* Python package, for amenity, shop, leisure, and tourism tags (POIs), building tags, and landuse tags.

Building and POI counts vary by more than two orders of magnitude across the network, from 7 to 2,234 landuse polygons and 11 to 592 POIs, reflecting the wide range of urban contexts from dense interchange catchments (Chatuchak, CTK: 592 POIs, 2,234 buildings) to sparse suburban catchments. RST and LHK, the two Thammasat proxy stations, occupy two of the three sparsest catchments on the network by building count (RST: 30 buildings, 40 POIs; LHK: 118 buildings, 11 POIs), despite RST's high operational volume (Cluster 2 in the volume-inclusive typology, Section 4.4.4) and LHK's university-adjacency.

Land-use composition (Table 16) shows both stations to be predominantly residential (RST 50%, LHK 57% of landuse polygons) with comparatively low green or open space share (RST 17%, LHK 14%, against a network median of approximately 35 to 50%). Neither station's land use polygons carry an education or institutional tag; the only stations with an institutional landuse polygon are Krung Thep Aphiwat (KTW) and Chatuchak (CTK), both unrelated to Thammasat.

However, inspection of the POI layer reveals that LHK's institutional adjacency is real, but is captured under amenity tags rather than landuse. Among LHK's 11 POIs is an amenity=university entry identifying Rajamangala University of Technology Thanyaburi (RMUTT), Rangsit Campus, together with a primary school (amenity=school). This indicates that LHK's university-adjacency, the basis for its selection as a behavioural proxy in Section 4.3, is confirmed by the spatial data, but that this characteristic is not visible in landuse polygon composition alone. RST's POIs, by contrast, are dominated by transport-support functions (three bus_station entries, a fuel station cluster, a parking area, and railway ticketing points), alongside two schools and a hospital, consistent with its role as a terminus and transfer point rather than a campus-adjacent station.

Table 16*. Land-use composition (residential, green/open, commercial/retail, institutional shares) and POI/building counts within a 1 km radius, all thirteen SRT Red Line Phase I stations. Note: institutional adjacency (e.g. university campuses) may be present as point-of-interest entries even where the institutional share of land-use polygons is zero.*

Station	Buildings	POIs	Land use polygons	Residential (%)	Green/open (%)	Commercial/ retail (%)	Institutional (%)
TLC	104	22	94	36	49	3	0
BMR	162	145	16	56	12	19	0
BSN	141	55	61	54	23	16	0
KTW	1204	481	122	13	50	28	1
CTK	2234	592	120	9	51	32	1
WSN	577	214	83	19	70	5	0
BKH	604	324	73	25	66	3	0
TSH	195	89	45	31	51	9	0
LAK	1045	97	44	45	20	16	0
KHA	691	57	17	47	35	0	0
DMG	153	261	29	21	66	3	0
LHK	**118**	**11**	**7**	**57**	**14**	**14**	**0**
RST	**30**	**40**	**18**	**50**	**17**	**11**	**0**

This result refines, rather than complicates, the composite "university-adjacent, terminus-proximate" characterisation proposed for Thammasat in Section 4.4.3. LHK's university-adjacency is spatially confirmed, but manifests as a small number of discrete institutional POIs within an otherwise sparse, predominantly residential 1 km catchment, rather than as a distinct land-use category in its own right. If Thammasat's actual catchment exhibits a similar pattern, a sparse residential surrounding with one or more major institutional POIs at its margin, this would support the LHK-based moderation effect proposed for Thammasat's demand profile. A methodological note follows from this: land-use polygon counts alone may understate institutional presence near a station, and POI-level inspection (specifically amenity tags) should be retained as a necessary complement in any future spatial catchment analysis of this kind, including for Thammasat itself once site-specific data become available. Should Thammasat’s catchment prove markedly denser than either proxy once data become available, this would represent a further point of divergence from the typological basis established in Sections 4.3 and 4.4, and is noted in the Discussion (Section 5).

4.5 Climate stress-testing: Heat Index projections and the catchment-shrinkage mechanism

The scenarios analysed in Sections 4.1 to 4.2 and the empirical and typological analyses in Sections 4.3 and 4.4 are based on present-day demand patterns. This section introduces a climate dimension: it asks how the thermal environment surrounding the station is projected to change over the coming decades, and what this implies for

the demand-concentration mechanisms already identified, particularly the SC-05 and SC-06 scenarios and the Skywalk Concourse's role as a passive crowd buffer (Section 4.2).

4.5.1 Heat Index methodology and data sources

Outdoor thermal stress was characterised using the Rothfusz Heat Index, computed from near-surface air temperature and relative humidity, with values reported only where temperature exceeds 27 degrees Celsius and relative humidity exceeds 40%, the validity range of the Rothfusz formulation. Two data sources were used. First, ERA5 reanalysis (1990 to 2024) provided an observationally-constrained historical baseline, at approximately 31 km spatial resolution, with relative humidity derived from 2 m temperature and 2 m dewpoint temperature via the Magnus formula. Second, CMIP6 climate model projections (2015 to 2050) provided future trends, using three models (ACCESS-CM2, IPSL-CM6A-LR, and MPI-ESM1-2-LR) under two emissions pathways, SSP2-4.5 (moderate mitigation) and SSP5-8.5 (high emissions), with relative humidity derived from near-surface specific humidity and surface pressure. For both data sources, all variables were spatially averaged over a bounding box covering the Bangkok Metropolitan Region and the Thammasat station site prior to Heat Index calculation. CMIP6 grid coverage over this area is sparse, ACCESS-CM2 provides 2 grid points, IPSL-CM6A-LR and MPI-ESM1-2-LR provide 1 grid point each, which limits spatial precision but is unavoidable given the native resolution of these models (approximately 100 to 250 km).

Annual mean Heat Index was computed for each model, experiment, and the ERA5 baseline. Because the validity mask produces occasional missing years where mean conditions fall outside the formula's valid range, a 5-year centred rolling mean (minimum 3 valid years per window) was applied to all series before constructing a three-model ensemble for each emissions pathway, reported as an ensemble mean with a minimum to maximum range across the three models.

4.5.2 Observed baseline and projected trends

The ERA5 baseline shows a 1990 to 2024 annual mean Heat Index of approximately 32.5 degrees Celsius (5-year smoothed value rising from 32.56 degrees Celsius in 1990 to 33.31 degrees Celsius in 2024). The CMIP6 ensemble projects a continued, modest warming trend to 2050 (Table 17). Under SSP2-4.5, the ensemble mean Heat Index rises from 31.1 degrees Celsius in 2030 (range 30.7 to 31.6 degrees Celsius across the three models) to 32.0 degrees Celsius in 2050 (range 31.7 to 32.4 degrees Celsius). Under SSP5-8.5, the ensemble mean rises from 31.5 degrees Celsius in 2030 (range 30.7 to 32.2 degrees Celsius) to 32.0 degrees Celsius in 2050 (range 30.9 to 33.4 degrees Celsius), representing an increase of approximately 0.9 degrees Celsius in the ensemble mean over the 20-year period. The two emissions pathways remain close together until approximately 2035, after which SSP5-8.5 diverges to higher values, consistent with the expectation that emissions pathways separate meaningfully only after mid-century. Model spread widens toward 2050, particularly under SSP5-8.5, reflecting compounding uncertainty further into the projection period.

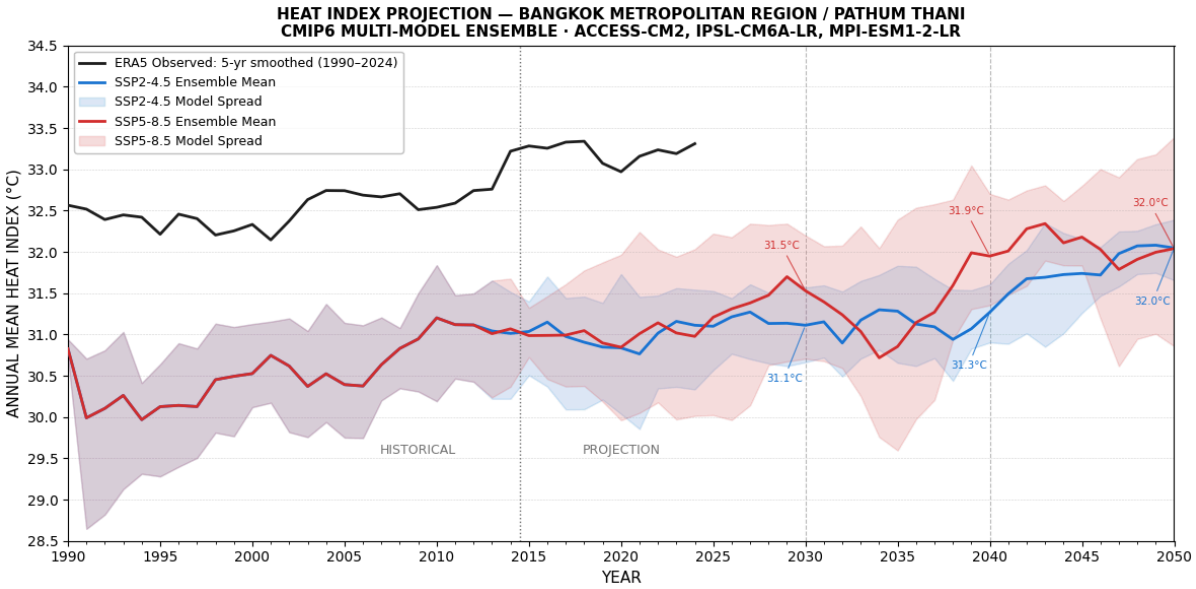

Figure 10. *Heat Index projections to 2050, showing ERA5 observed (5-year smoothed, 1990 to 2024) and CMIP6 three-model ensemble means and ranges for SSP2-4.5 and SSP5-8.5 (2015 to 2050), with 2030, 2040, and 2050 milestones annotated.*

Table 17. *CMIP6 three-model ensemble mean Heat Index (degrees Celsius), with model range, for 2030, 2040, and 2050 under SSP2-4.5 and SSP5-8.5.*

Milestone year	SSP2-4.5 ensemble mean (range)	SSP5-8.5 ensemble mean (range)
2030	31.1 (30.7 to 31.6)	31.5 (30.7 to 32.2)
2040	31.3 (30.9 to 31.6)	31.9 (31.4 to 32.7)
2050	32.0 (31.7 to 32.4)	32.0 (30.9 to 33.4)

4.5.3 The ERA5 to CMIP6 offset: a methodological transparency note

Throughout the overlapping period, the ERA5 baseline sits approximately 1.5 to 2 degrees Celsius above the CMIP6 ensemble. This offset is treated here as a known limitation of coarse-resolution global climate models over tropical urban areas, rather than a processing error, for four compounding reasons. First, a resolution mismatch: CMIP6 grid cells of approximately 100 to 250 km blend the Bangkok Metropolitan Region with surrounding agricultural land, wetlands, and coastline into a single averaged value, whereas ERA5's approximately 31 km grid, constrained by assimilated observations, captures the local thermal signature more faithfully. Second, the urban heat island effect of one of Southeast Asia's most intensely urbanised regions is largely absent from CMIP6's parameterisation, while ERA5 implicitly captures it through assimilation against in-city station observations. Third, coarse models tend to over-represent convective mixing in tropical climates, ventilating heat away from the surface more efficiently than occurs in a dense urban environment, producing a systematic cool and dry bias in the boundary layer. Fourth, because the Heat Index responds non-linearly to the combination of temperature and humidity, a model that runs simultaneously cool and dry produces a Heat Index deficit larger than either bias would suggest individually.

The practical implication is that ERA5 provides the observationally-constrained baseline, while CMIP6 provides the trend signal: the absolute projected values are less trustworthy than the direction and rate of change they describe. Accordingly, the 2030 to 2050 milestones in Table 17 are presented, and should be interpreted, as indicators of the magnitude and pacing of future warming relative to the CMIP6 historical baseline, rather than as absolute Heat Index forecasts for the station site. This framing is consistent with standard practice in climate impact studies, where bias-corrected or anomaly-based projections are preferred over raw model output, and is presented explicitly here rather than addressed through bias correction, which was not applied.

4.5.4 From Heat Index to catchment shrinkage: a behavioural mechanism

The climate projections in Sections 4.5.2 and 4.5.3 describe the thermal environment surrounding the station, but on their own do not speak to station operations. The analytical bridge proposed here rests on a single behavioural hypothesis: as outdoor Heat Index rises, pedestrians minimise exposed walking distance, contracting their effective walking catchment around the station and concentrating arrivals toward the nearest available access point.

This hypothesis connects directly to the demand-concentration scenarios already examined in Section 4.2. SC-05 (network platooning) and SC-06 (stadium impulse load) modelled the operational consequences of concentrated arrival demand at the station, finding that the Skywalk Concourse absorbs such concentration as a passive buffer, reaching maximum occupancy of 415 pax under SC-06 while remaining at PLOS B (Section 4.2.2, Table 8). In both SC-05 and SC-06, the concentration of demand was modelled as an exogenous event, a network delay or a stadium egress, occurring independently of ambient conditions. The Heat Index projections in Section 4.5.2 suggest a complementary, climatically-driven concentration mechanism operating on a longer timescale: as the annual mean Heat Index rises from its current baseline of approximately 32.5 degrees Celsius toward the 2040 to 2050 range of approximately 31.3 to 32.0 degrees Celsius (SSP2-4.5) or 31.9 to 32.0 degrees Celsius (SSP5-8.5), with corresponding increases in the frequency and severity of individual extreme-heat days beyond these annual means, the proportion of passengers whose walking catchment contracts toward the station's nearest entrance may increase correspondingly.

If this mechanism operates as hypothesised, the demand concentration modelled in SC-05 and SC-06 would by 2040 to 2050 increasingly reflect a standing climatic condition rather than an occasional disruption. The 2040 to 2050 window, in which the SSP5-8.5 ensemble mean Heat Index approaches and the SSP2-4.5 mean reaches 32.0 degrees Celsius, is proposed as a critical planning horizon on this basis, and is discussed further in Section 5.3.

This mechanism also bears directly on the Skywalk Concourse's function as a passive crowd buffer (Section 4.2.3) and on the architectural and typological findings of Section 4.4. If climatically-driven catchment shrinkage concentrates arrivals toward a station's nearest entrance, the spatial distribution of access points examined in Section 4.4.5 becomes directly relevant: a distributed, multi-node station such as RST may experience this concentration effect at multiple points simultaneously, each individually less severe, whereas a concentrated, two-cluster station such as LHK may experience a more acute concentration at whichever of its two clusters is nearest to the bulk of the contracting catchment. For Thammasat, whose access topology remains an open question (Section 4.4.5), this represents a further dimension along which the station's architectural configuration may interact with its climate exposure.

4.5.5 Limitations

Three limitations apply to this analysis. First, the behavioural hypothesis linking Heat Index to catchment contraction is presented as a plausible mechanism grounded in established pedestrian behaviour literature on thermal comfort and walking distance, but has not been empirically tested against observed ridership data for this study; the OD dataset described in Section 4.3 covers a single year (June 2025 to May 2026) and was not analysed for Heat Index sensitivity, a natural extension for future work. Second, the CMIP6 ensemble's sparse spatial coverage (1 to 2 grid points per model) and the ERA5 to CMIP6 offset discussed in Section 4.5.3 mean that the absolute Heat Index values, and by extension the precise timing of the 2040 to 2050 critical window, carry meaningful uncertainty; the qualitative direction of the trend is considered more robust than its exact magnitude or timing. Third, the analysis considers only annual mean Heat Index; the operationally relevant quantity for pedestrian behaviour is more likely the frequency and intensity of individual extreme-heat days, which may increase disproportionately relative to the annual mean and would require daily-resolution CMIP6 output to characterise, also identified as a priority for future work.

Taken together, the climate analysis adds a third strand to the picture built across this section. Section 4.2 established that the station's architecture, particularly the Skywalk Concourse, absorbs concentrated demand as a passive buffer under exogenous disruptions. Section 4.3 found that present-day peak-hour demand concentration already exceeds the levels assumed in the Machinations model. Section 4.4 positioned Thammasat, on the basis of demand shape, volume, architecture, and spatial catchment, as most closely resembling RST's terminus-driven profile, with a secondary moderating influence from LHK's university-adjacency. The climate findings in this section suggest that the gap between assumed and observed demand concentration identified in Section 4.3, and the buffering capacity characterised in Section 4.2, should not be evaluated only against current conditions. By the 2040 to 2050 period, a climatically-driven contraction of walking catchments may render the concentrated-demand conditions of SC-05 and SC-06 closer to typical operating conditions than to occasional disruptions, a possibility that depends on the station's access topology (Section 4.4.5) and reinforces the case, raised throughout Sections 4.3 and 4.4, for revisiting the demand assumptions underlying SC-02, SC-05, and SC-06 specifically for the Thammasat site.

5. Discussion and Limitations

5.1 Synthesis: a dichotomy of resilience

The results presented in Section 4 reveal a consistent dichotomy in the Thammasat station archetype's operational resilience. Against external, network-level disruption, the station is robust: SC-05 demonstrated that even a platooned, compounded train arrival following a 10-minute headway delay is absorbed by the vertical-circulation hardware without materially affecting the Skywalk Concourse, indicating that this hardware is over-engineered relative to the railway-induced disruptions it is likely to face in practice. Against internal hardware degradation, however, the station's resilience is uneven and orientation-dependent. The AFC gate array, a horizontal, parallel arrangement, tolerates a 33% capacity loss (SC-03) with negligible degradation, the remaining gates simply absorb the diverted flow. The escalator-to-stair failover (SC-04), by contrast, is the single most severe degradation pathway tested, nearly doubling platform clearance time and pushing platform LOS to C, the only scenario in this study to do so. This asymmetry, horizontal redundancy versus vertical vulnerability, is a structural property of the station's circulation topology rather than an artefact of any single scenario, and is consistent with the thesis's original finding that kinematic stairwell egress, not ticketing throughput, is the binding constraint on station-wide resilience.

The Skywalk Concourse's role as a passive crowd buffer (Section 4.2) sits alongside this dichotomy as the study's central architectural finding. Under both the most severe internal failure (SC-04, 446 pax) and the most severe exogenous load (SC-06, 415 pax), the concourse absorbed spatial accumulation that would otherwise have reached the platform, in every tested case remaining at or below PLOS B. This buffering is not the product of deliberate crowd-management design; it emerges from the interaction between throttled downward capacity (escalators, AFC gates) and the concourse's unhindered architectural width. The practical implication, consistent with the thesis's policy recommendation, is that horizontal concourse width above an active guideway may represent a safety-critical design parameter in future station archetypes, warranting consideration alongside passenger-comfort criteria rather than as an afterthought to them.

5.2 Reframing demand assumptions in light of the empirical and typological evidence

The empirical validation in Section 4.3 complicates the resilience picture established above in an important way. All thirteen operating Phase I stations, including both Thammasat proxies, exhibit peak-hour demand shares that exceed the Machinations model's assumed k-factors (12% AM, 10% PM), in some cases substantially: Rangsit's observed AM share (20.3%) is approximately 1.7 times the assumed value. Because every stress-test scenario in Section 4.1 and 4.2 was generated using these assumed k-factors, the SC-02, SC-05, and SC-06 results should be read as a lower bound on Thammasat's likely peak-hour demand concentration, not a central estimate. The analytical sensitivity check in Section 4.2.4 provides a first, necessarily approximate, answer to this question for

SC-06: the Skywalk Concourse's buffering capacity holds at PLOS B at the lower end of the empirical k-factor range (15% AM) but degrades to PLOS C at the upper end (20% AM). Rangsit's own observed AM share of 20.3% sits at, and marginally above, this upper bound, the precise figure this sensitivity check identifies as the point at which the concourse buffer is no longer maintained at PLOS B or better. Because Rangsit is also the closest network-position proxy for Thammasat's prospective terminus role (Section 4.4.3), this is not a hypothetical edge case: it is closer to the demand condition Thammasat may plausibly inherit than the 12% AM figure the core simulation matrix assumes. Given that SC-04 already identifies escalator failure as the binding constraint under assumed demand, and that the Skywalk buffer itself shows degradation under empirically realistic peaking, a full stochastic re-simulation of the stress-test matrix under empirically-calibrated demand, extending the preliminary analytical check in Section 4.2.4 to all six scenarios and restoring proper Monte Carlo treatment, is a priority before any operational policy is finalised.

The typology analysis (Section 4.4) adds a further layer of nuance rather than resolving this gap. Because Rangsit and Lak Hok, the two best available behavioural proxies, fall into different demand-shape clusters (Directional/Terminus-like and Balanced/Interchange-like respectively), and because volume-inclusive clustering reshuffles both stations into still different groups, there is no single, unambiguous archetype that Thammasat can be assumed to inherit. The working hypothesis developed in Section 4.4.3, a terminus-driven profile moderated by a university-adjacency effect, is a reasoned interpolation between two structurally dissimilar proxies rather than a directly observed pattern, and should be treated accordingly in any operational planning that relies on it. The implications of this typology ambiguity for operational and capital-planning decisions are discussed in Section 5.2.

5.3 The climate dimension: from occasional disruption to standing condition

Section 4.5's climate analysis reframes the relationship between the demand-concentration scenarios (SC-05, SC-06) and time. If the catchment-shrinkage mechanism operates as hypothesised, by the 2040 to 2050 period, particularly under SSP5-8.5, the concentrated-arrival conditions currently modelled as exceptional disruptions may increasingly describe typical operating conditions during the hottest months of the year. This has a direct implication for the Skywalk Concourse's buffering role: a mechanism currently relied upon for occasional, bounded events (a stadium egress, a network delay) may need to perform that function routinely. Because the buffer's capacity is fixed by architecture rather than by operational policy, this is, in effect, a long-horizon early-warning signal rather than an immediate operational concern, and is best read as a planning input for any future expansion or renovation decision rather than a call for near-term intervention.

The interaction between this climate mechanism and the station's access topology (Section 4.4.5) is worth flagging explicitly. A distributed, multi-node access pattern (RST-like) would likely absorb climatically-driven catchment contraction more gracefully than a concentrated, two-cluster pattern (LHK-like), since contracting demand would redistribute across several entry points rather than concentrating at one. Resolving which pattern Thammasat will follow, currently an open question pending site-specific architectural drawings, therefore has a bearing not only on present-day operations but on the station's exposure to this longer-term climatic mechanism.

5.4 Operational recommendations

Three operational interventions follow directly from the findings above, consistent with and extending the thesis's original recommendations. First, active gate metering: deliberately throttling AFC gate throughput during anticipated impulse loads (a scheduled stadium event, for example) would intentionally route accumulation into the Skywalk Concourse rather than allowing it to reach the platform unmetered, operationalising a behaviour the simulation shows occurs passively under SC-06. Second, dynamic hardware reversal: reversing a downward escalator to prioritise the alighting AM-peak surge during an SC-04-type failure would partially offset the kinematic penalty of stair-only egress, a low-cost mitigation requiring no structural change. Third, and most directly motivated by the empirical findings in Section 4.3, the k-factor assumptions underlying the simulation should be revisited using the empirically-derived range (15 to 20% AM, 12 to 15%

PM) identified in this study, rather than the original planning assumptions, before any of the above interventions are sized for operational deployment.

5.5 Limitations

This study is subject to limitations across each of its analytical strands. The simulation core inherits the macroscopic abstractions of the original thesis: Machinations processes passenger volumes as discrete numeric transfers and does not capture microscopic crowd behaviours such as localised pushing or panic response, and the model assumes uniform kinematic profiles, omitting passengers with reduced mobility, heavy luggage, or cohesive group movement, any of which would increase effective processing friction beyond what is simulated here. The model also assumes unhindered train dwell time, whereas platform crowding at LOS B or C in practice can extend dwell by obstructing door closure, a feedback loop not captured at this resolution. The AnyLogic cross-validation (Section 3.5) introduces a further scope limitation: by isolating the Skywalk Concourse to platform transition rather than replicating the full station, it does not capture potential upstream bottlenecks, such as queuing at street-level entrances or friction at the AFC turnstiles themselves, that could alter the arrival distribution actually reaching the modelled node. Because the cross-validation's arrival rates are taken directly from the Machinations model rather than generated independently within AnyLogic, this scope choice does not affect the cross-validation's internal consistency, but it does mean that any upstream congestion not represented in the Machinations model would also be absent from this study's microscopic results.

The empirical validation and typology analyses are constrained by the available proxy stations: Rangsit and Lak Hok are the best structural analogues on the existing network, but neither is a perfect match for a station that will be simultaneously a line terminus and a major university access point, a combination not otherwise present in the current thirteen-station network. These same two stations underpin both the k-factor validation in Section 4.3 and the typology classification in Section 4.4; the two analyses are therefore related rather than fully independent lines of evidence, and a structural peculiarity specific to either station, rather than a genuine feature of the terminus or university-adjacent archetype it is taken to represent, could propagate into both findings simultaneously. The twelve-month OD dataset, while comprehensive, covers a single year and was not tested for sensitivity to ambient temperature or Heat Index, which would be necessary to empirically ground the catchment-shrinkage mechanism proposed in Section 4.5 rather than treat it as a plausible but untested hypothesis. The climate projections themselves carry meaningful uncertainty: the CMIP6 ensemble's sparse spatial coverage and the documented ERA5 to CMIP6 offset (Section 4.5.3) mean that the qualitative direction of warming is more robust than its precise magnitude or timing, and the analysis considers only annual mean Heat Index rather than the frequency of individual extreme-heat days, which is likely the more behaviourally relevant quantity.

5.6 Directions for future work

Several extensions follow naturally from the limitations above. Re-running the six stress-test scenarios under the empirically-derived k-factors from Section 4.3, rather than the original planning assumptions, is the most immediate priority, since it would directly test whether the SC-04 escalator vulnerability and the SC-06 buffer capacity remain adequate under realistic rather than assumed peak demand. Testing the OD dataset for Heat Index sensitivity, once a second year of data becomes available, would allow the catchment-shrinkage hypothesis in Section 4.5.4 to move from a plausible mechanism to an empirically grounded one. Heterogeneous agent-based modelling in AnyLogic, extending beyond the single bottleneck node already cross-validated, would relax the homogeneous kinematic assumption and provide a more rigorous test of the Skywalk buffer's capacity under a more realistic passenger mix. Finally, once architectural drawings for the Thammasat station itself become available, the open question of its access topology, distributed and RST-like, or concentrated and LHK-like, raised in Sections 4.4.5 and 5.3, can be resolved directly rather than inferred from proxy stations.

6. Conclusion

This study presented a pre-operational, multi-strand evaluation of the planned Thammasat University station on the SRT Red Line Phase II extension, combining a dual-tier hybrid simulation, empirical demand validation, station typology classification, and climate stress-testing within a single analytical framework.

The dual-tier simulation, a macroscopic Machinations model cross-validated against a microscopic AnyLogic pedestrian engine, established that the station's architecture performs within acceptable Pedestrian Level of Service bounds under nominal peak loading and most tested disruptions. Resilience, however, is uneven: horizontal AFC capacity tolerates substantial loss with negligible degradation, while vertical circulation, specifically escalator failure, is the binding constraint on station-wide performance. The most significant finding to emerge from this analysis is that the Skywalk Concourse functions as a passive crowd buffer, absorbing spatial accumulation under both the most severe internal failure and the most severe exogenous impulse load tested, in every case remaining within an operationally acceptable Level of Service. This behaviour arises from the interaction between throttled vertical-circulation capacity and the concourse's architectural width, rather than from any active crowd-management design, and constitutes the study's primary contribution to station-level resilience planning.

The empirical and typological extensions situate this simulation-based finding within observed network behaviour. Validation against twelve months of operational origin-destination data from the existing Red Line network showed that the Machinations model's peak-hour demand assumptions are conservative relative to every one of the thirteen currently operating stations, with the two closest behavioural proxies for Thammasat exceeding the assumed k-factors by 26 to 70%. Station typology classification further showed that these two proxies, despite both being plausible analogues for Thammasat, fall into structurally different demand archetypes, indicating that network position rather than university-adjacency alone governs temporal demand concentration on this line. Together, these findings indicate that the stress-test results in Section 4 should be read as a lower bound on the demand-concentration conditions Thammasat is likely to face, and that the buffering capacity identified above, while currently adequate, was tested against assumptions now shown to understate observed peak-hour behaviour.

The climate stress-testing extension adds a temporal dimension to this picture. Heat Index projections to 2050, anchored to an ERA5 observational baseline and informed by a three-model CMIP6 ensemble, suggest a plausible mechanism by which rising ambient heat could compress commuters' effective walking catchment, concentrating arrivals toward the station in a manner analogous to the concentrated-demand scenarios already modelled. Under the high-emissions pathway, this mechanism may render such concentrated conditions closer to typical than exceptional by mid-century, a finding that bears directly on the continued adequacy of the Skywalk Concourse's buffering role over the station's operational lifetime.

Taken together, these four strands support a central conclusion: passive architectural features, specifically generous, unhindered horizontal circulation space, can provide substantial and currently underappreciated resilience against both engineered and climatic stressors. These findings suggest that passive architectural width may represent a transferable, safety-relevant design parameter for future transit-oriented station archetypes, particularly those serving university-adjacent or otherwise demand-concentrated catchments, though this transferability remains to be confirmed through investigation across additional station typologies and site conditions. The methodology demonstrated here, a dual-tier simulation grounded and stress-tested against empirical network data, typological context, and climate projection, offers a candidate framework for pre-operational resilience assessment at other planned stations on the SRT network and in comparable tropical, transit-oriented contexts more broadly.

Acknowledgements

The authors wish to thank the State Railway of Thailand for providing access to the anonymised origin-destination passenger dataset that forms the empirical foundation of this study's validation analysis. The simulation and analysis were conducted independently, and the findings, interpretations, and conclusions expressed in this paper are those of the authors alone and do not represent the official position of the State Railway of Thailand or any affiliated institution.

Data availability

All derived datasets, geospatial data, tabular outputs, analysis code, and the simulation model in AnyLogic supporting this study are openly available on Zenodo at https://doi.org/10.5281/zenodo.20785876 under a Creative Commons Attribution 4.0 International licence. Station architectural floor plans used for spatial cross-checking in this study are not included in this deposit due to redistribution restrictions; interested parties should request these directly from the State Railway of Thailand. The Machinations model is publicly available at https://my.machinations.io/d/gravitymodelpassenger/cb91d44f46b111f190390abc5ce0dcc9. The simulation model was implemented in AnyLogic 8 (Personal Learning Edition, version 8.9.8). Raw climate input data are publicly available from their respective providers: ERA5 monthly averaged reanalysis data on single levels, Copernicus Climate Data Store (https://doi.org/10.24381/cds.f17050d7), and CMIP6 model output (ACCESS-CM2, IPSL-CM6A-LR, MPI-ESM1-2-LR; variant r1i1p1f1; historical, SSP2-4.5, and SSP5-8.5 experiments), Earth System Grid Federation (https://esgf-node.llnl.gov/projects/cmip6/). Processed climate derivatives generated for this study are included in the Zenodo deposit above. Empirical analysis, spatial extraction, and visualisation were conducted in Python 3 using pandas, numpy, scikit-learn, matplotlib, seaborn, scipy, xarray, and osmnx.

Declaration of Competing Interest

The authors declare that there are no conflicts of interest with respect to the research, authorship, or publication of this article. No financial or personal relationships with any organisation or individual have influenced the work reported herein. This research received no external funding.

Ethics Statement

This research did not involve human participants, animal subjects, or any form of clinical intervention. The origin-destination dataset used to empirically validate the simulation's demand assumptions was obtained from the State Railway of Thailand under a formal data governance agreement and was fully anonymised prior to analysis; no personally identifiable information is present in the dataset or reported in this article. Accordingly, ethical approval was not required and is not applicable to this study.

References

[1] J.I.C.A. (JICA) Department of Rail Transport (DRT), *The Project for Enhancing Capacity of Formulation of the Second Mass Rapid Transit Master Plan in Bangkok Metropolitan Region (M-MAP2) in the Kingdom of Thailand*. Ministry of Transport, Thailand, 2024.

[2] Bangkok Post, "Bidding for Red Line extensions begins," *Bangkok Post*, Dec. 2, 2025. Available: https://www.bangkokpost.com/thailand/general/3148145/bidding-for-red-line-extensions-begins

[3] P. Iamtrakul and S. Chayphong, "Exploring Spatial Accessibility to Urban Activities Based on the Transit-Oriented Development Concept in Pathum Thani, Thailand," *Sustainability*, vol. 16, no. 5, p. 2195, Jan. 2024, doi: 10.3390/su16052195.

[4] M. Seehamart, S. Pueboobpaphan, and R. Pueboobpaphan, "Actual walking distance vs. Perceived walking distance: Relationship and impact on determining acceptable walking distances to stations of the Bangkok Metro," *Results Eng.*, vol. 25, p. 104088, Mar. 2025, doi: 10.1016/j.rineng.2025.104088.

[5] Ecology, Community, and the American Dream, "'The Next American Metropolis': from *The Next American Metropolis* (1993), Peter Calthorpe," in *The Sustainable Urban Development Reader*, Routledge, 2004.

[6] R. Cervero and D. Dai, "BRT TOD: Leveraging transit oriented development with bus rapid transit investments," *Transp. Policy*, vol. 36, pp. 127–138, Nov. 2014, doi: 10.1016/j.tranpol.2014.08.001.

[7] L. Bertolini, "Spatial Development Patterns and Public Transport: The Application of an Analytical Model in the Netherlands," *Plan. Pract. Res.*, vol. 14, no. 2. Available: https://www.tandfonline.com/doi/abs/10.1080/02697459915724

[8] A. El-Geneidy, M. Grimsrud, R. Wasfi, P. Tétreault, and J. Surprenant-Legault, "New evidence on walking distances to transit stops: identifying redundancies and gaps using variable service areas," *Transportation*, vol. 41, no. 1, pp. 193–210, Jan. 2014, doi: 10.1007/s11116-013-9508-z.

[9] J. Gutiérrez, O. D. Cardozo, and J. C. García-Palomares, "Transit ridership forecasting at station level: an approach based on distance-decay weighted regression," *J. Transp. Geogr.*, vol. 19, no. 6, pp. 1081–1092, Nov. 2011, doi: 10.1016/j.jtrangeo.2011.05.004.

[10] G. K. Zipf, "The P1 P2/D Hypothesis: On the Intercity Movement of Persons," *Am. Sociol. Rev.*, vol. 11, no. 6, pp. 677–686, 1946, doi: 10.2307/2087063.

[11] W. G. Hansen, "How Accessibility Shapes Land Use," *J. Am. Inst. Plann.*, vol. 25, no. 2, pp. 73–76, May 1959, doi: 10.1080/01944365908978307.

[12] A. G. Wilson, "A statistical theory of spatial distribution models," *Transp. Res.*, vol. 1, no. 3, pp. 253–269, Nov. 1967, doi: 10.1016/0041-1647(67)90035-4.

[13] J. J. Fruin, "Pedestrian Planning and Design," 1971. Available: https://trid.trb.org/View/114653

[14] M. Kobes, I. Helsloot, B. de Vries, and J. Post, "Exit choice, (pre-)movement time and (pre-)evacuation behaviour in hotel fire evacuation," *Procedia Eng.*, vol. 3, pp. 37–51, Jan. 2010, doi: 10.1016/j.proeng.2010.07.006.

[15] R. Daniels and C. Mulley, "Explaining walking distance to public transport: The dominance of public transport supply," *J. Transp. Land Use*, vol. 6, no. 2, pp. 5–20, Aug. 2013, doi: 10.5198/jtlu.v6i2.308.

[16] R. Pueboobpaphan, S. Pueboobpaphan, and S. Sukhotra, "Acceptable walking distance to transit stations in Bangkok, Thailand: Application of a stated preference technique," *J. Transp. Geogr.*, vol. 99, p. 103296, Feb. 2022, doi: 10.1016/j.jtrangeo.2022.103296.

[17] R. Cervero, O. L. Sarmiento, E. Jacoby, L. F. Gomez, and A. Neiman, "Influences of Built Environments on Walking and Cycling: Lessons from Bogotá," *Int. J. Sustain. Transp.*, vol. 3, no. 4, pp. 203–226, Jun. 2009, doi: 10.1080/15568310802178314.

[18] H. Zhang, B. He, G. Lu, and Y. Zhu, "A simulation and machine learning based optimization method for integrated pedestrian facilities planning and staff assignment problem in the multi-mode rail transit transfer station," *Simul. Model. Pract. Theory*, vol. 115, p. 102449, Feb. 2022, doi: 10.1016/j.simpat.2021.102449.

[19] S. Seriani and R. Fernandez, "Pedestrian traffic management of boarding and alighting in metro stations," *Transp. Res. Part C Emerg. Technol.*, vol. 53, pp. 76–92, Apr. 2015, doi: 10.1016/j.trc.2015.02.003.

[20] T. Murata, "Petri nets: Properties, analysis and applications," *Proc. IEEE*, vol. 77, no. 4, pp. 541–580, Apr. 1989, doi: 10.1109/5.24143.

[21] A. M. Law, *Simulation Modeling and Analysis*, 5th ed. New York, NY, USA: McGraw-Hill Education, 2014. Available: https://www.mheducation.com/highered/product/simulation-modeling-and-analysis-law.html

[22] M.A. Young, S.P. Blainey, T. Gowland, and S. Nagella, "An automated online tool to forecast demand for new railway stations and analyse potential abstraction effects," University of Southampton / DAFNI. Available: https://eprints.soton.ac.uk/432493/

[23] L. Pang, Y. Jiang, J. Wang, N. Qiu, X. Xu, L. Ren, and X. Han, "Research of Metro Stations with Varying Patterns of Ridership and Their Relationship with Built Environment, on the Example of Tianjin, China," *Sustainability*, vol. 15, no. 12, p. 9533, 2023, doi: 10.3390/su15129533.

[24] L.P. Rothfusz, "The Heat Index Equation (or, more than you ever wanted to know about heat index)," NWS Technical Attachment SR 90-23, National Weather Service, Fort Worth, Texas, 1990. Available: https://www.weather.gov/media/ffc/ta_htindx.PDF

[25] H. Hersbach et al., "The ERA5 global reanalysis," *Q. J. R. Meteorol. Soc.*, vol. 146, no. 730, pp. 1999–2049, 2020, doi: 10.1002/qj.3803.

[26] V. Eyring et al., "Overview of the Coupled Model Intercomparison Project Phase 6 (CMIP6) experimental design and organisation," *Geosci. Model Dev.*, vol. 9, pp. 1937–1958, 2016, doi: 10.5194/gmd-9-1937-2016.

[27] Q. Kong and M. Huber, "A global high-resolution and bias-corrected dataset of CMIP6 projected heat stress metrics," *Sci. Data*, vol. 12, art. 246, 2025, doi: 10.1038/s41597-025-04527-6.